HHS Public Access

Author manuscript

J Colloid Interface Sci. Author manuscript; available in PMC 2019 July 01.

Published in final edited form as:

J Colloid Interface Sci. 2018 July 01; 521: 261–279. doi:10.1016/j.jcis.2018.02.053.

Multifunctional Nanomedicine with Silica: Role of Silica in Nanoparticles for Theranostic, Imaging, and Drug Monitoring

Fang Chen[1,2], **Ghanim Hableel**[1], **Eric Ruike Zhao**[1], and **Jesse V. Jokerst**[1,2,3,*]

[1]Department of NanoEngineering, University of California, San Diego, 9500 Gilman Drive, La Jolla, CA 92093, USA

[2]Materials Science and Engineering Program, University of California, San Diego, 9500 Gilman Drive, La Jolla, CA 92093, USA

[3]Department of Radiology, University of California, San Diego, 9500 Gilman Drive, La Jolla, CA 92093, USA

Abstract

The idea of multifunctional nanomedicine that enters the human body to diagnose and treat disease without major surgery is a long-standing dream of nanomaterials scientists. Nanomaterials show incredible properties that are not found in bulk materials, but achieving multi-functionality on a single material remains challenging. Integrating several types of materials at the nano-scale is critical to the success of multifunctional nanomedicine device. Here, we describe the advantages of silica nanoparticles as a tool for multifunctional nano-devices. Silica nanoparticles have been intensively studied in drug delivery due to their biocompatibility, degradability, tunable morphology, and ease of modification. Moreover, silica nanoparticles can be integrated with other materials to obtain more features and achieve theranostic capabilities and multimodality for imaging applications. In this review, we will first compare the properties of silica nanoparticles with other well-known nanomaterials for bio-applications and describe typical routes to synthesize and integrate silica nanoparticles. We will then highlight theranostic and multimodal imaging application that use silica-based nanoparticles with a particular interest in real-time monitoring of therapeutic molecules. Finally, we will present the challenges and perspective on future work with silica-based nanoparticles in medicine.

Graphical abstract

*Correspondence and requests for materials should be addressed to jjokerst@ucsd.edu.

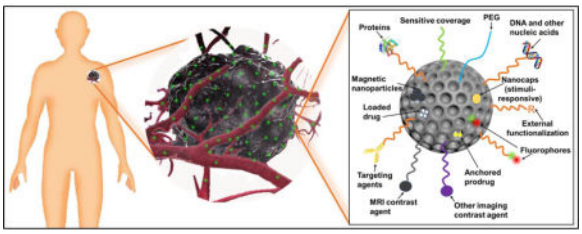

Keywords

nanomaterials; silica nanoparticles; multimodal imaging; theranostic; contrast agents; real-time molecules monitoring

1. Introduction

A microscopic system that can help doctors diagnose and treat diseases has fascinated the public and researchers since 1966. The emergence of nanotechnology in the 1980s pushed this dream closer to reality. Efforts towards building a multifunctional nanomedicine device include studies in multimodal imaging and theranostic nanomedicine[1]. These tools can diagnose patients using a variety of imaging modalities and can deliver cargo for imaging and/or therapy.

1.1 Definition and categories of nanomaterials

Nanomaterials are materials that have unique properties as a function of their intrinsic features smaller than 1000 nm. These materials typically differ in physical properties from bulk materials[2]. Nanomaterials that are popular in biology and medicine can be either man-made or natural. Man-made nanomaterials include carbon nanotubes[3–6], graphene[7–10], liposomes[11–14], dendrimers[15–19], polymers[20–26], silicon[27] and silicas[28–34] and other sol-gels[35], quantum dots[36–39], up-conversion nanoparticles (UCNPs)[40–44], superparamagnetic iron oxide nanoparticles[45–49], other metal oxides nanoparticles[50–53], and noble metals[54–58]. Natural nanomaterials used in nanomedicine are mainly deoxyribonucleic acid (DNA)[59–62]. In nanomedicine, these nanomaterials are commonly synthesized in the form of nanoparticles which range in size between one and several hundred nanometers[3, 63].

1.2 Properties of nanomaterials

Regardless of the underlying material, nanoparticles have a large surface area and high surface-to-volume ratio. These particles are comparable to the size of DNA plasmids, antibodies, enzymes, other biological macromolecules as well as cell products like exosomes[64] (Figure 1). This large surface area enables a high loading capacity of functional molecules such as therapeutics and imaging agents. Also, some nanoparticles have large porosity which is beneficial to high loading. Important factors that influence the nanoparticles' biodistribution include size, surface charge, dispersity, and hydrophobicity[65] (Figure 2). Generally, nanoparticles with a size smaller than 8 nm will be rapidly cleared by the kidneys. Larger nanoparticles between 30 to 200 nm can accumulate in tumors by the enhanced permeability and retention (EPR) effect[66]. The small size of nanoparticles also

benefits cell endocytosis[67, 68]. The surface properties are also important for nanoparticles because altering the surface chemistry of a nanoparticle will change its hydrodynamic size and surface charge as well as its reactivity (e.g., binding affinity).

Figure 2 shows that nanoparticles with positive surface charge are often more toxic because of complications such as hemolysis and platelet aggregation. Positively charged nanoparticles can also have shorter circulation half-lives than negative and neutral counterparts[66]. Hydrophobic nanoparticles will be rapidly cleared by the reticuloendothelial system (RES)[65].

While nanoparticles share a small size and high surface area, they differ in terms of the endogenous properties that govern their biocompatibility. The advantages and disadvantages as well as applications of various nanoparticles are presented in Table 1. Carbon nanotubes are pseudo one-dimensional nanomaterials that can penetrate through different cellular barriers. The high specific surface area and void in the center of carbon nanotubes can be used for drug delivery[3–6]. Graphene is a two-dimensional (2D) sheet of sp^2-hybridized carbon atoms packed into a honeycomb lattice. The high surface area gives graphene a high adsorption capacity for molecules[7–10].

Liposomes are spheres composed of lipid bilayer similar to biological membranes. Liposomes have been used to load cargos such as therapeutic molecules, nucleic acids, and fluorocarbon gas to achieve drug delivery, lipofection, and ultrasound contrast agents.[11–14] Dendrimers are highly branched polymers that can form nanoparticles with voids to load drugs and genes. Dendrimers can also be used as a blood substutite[15–19]. DNA origami utilizes the nanoscale folding of DNA and has been applied to drug delivery[59–62]. Quantum dots are luminescent zero-dimensional particles, and their photoluminescence can be manipulated to specific wavelengths by controlling the particle diameter[69]. They are commonly used in fluorescence/luminescence imaging[36–39].

UCNPs are nanoparticles that absorb two or more incident photons of relatively low energy[70]. These are then converted into one emitted photon with higher energy. These nanoparticles usually contain transition metals and are used for bio-imaging[40–44]. Superparamagnetic iron oxide nanoparticles have also been widely used as MRI contrast agents and manipulators combined with magnetic fields[45–49]. Other commonly investigated metal oxides nanoparticles include titanium oxide, zinc oxide, and manganese oxide (MnO) nanoparticles[50–52]. Noble metal nanoparticles are usually nanoscale particles composed of gold and/or silver, and these have surface plasmon resonance (SPR) that can enhance the sensitivity of several spectroscopic measurements such as fluorescence, Raman scattering, and second harmonics[71, 72]. Other emerging nanomedicines include fullerenes[73], nanoclays[74], and micelles[75].

1.3 Potential and challenges of nanomaterials in medicine

Nanomedicine based on the above nanomaterials has been reported to improve the medical imaging and treatment of various diseases, such as cancers[79–82], degenerative diseases[83, 84], heart disease[85, 86], diabetes[87, 88], and toxin detection[89]. Some nanomaterials are commercially available for their medical applications. For example, Abraxane, Doxil, and

Megace ES are Food and Drug Administration (FDA)-approved nanotechnology-based drugs used to treat cancers[80]. Moreover, there are many nanomaterials that are currently in clinical trials. For instance, Cornell Dots (C-dots) are a nanoparticle-based diagnostic tool that is used for imaging tumors[90] and currently in clinical trials. However, these commercial nanosystems have only one function.

Indeed, diagnosis and therapy are currently two separate steps. Multiple nanosystems are needed if each nanosystem can only perform one of those functions, but can results in problems with interference and dosage. First, nanosystems may interfere with each other causing unexpected side effects or decreasing the diagnostic and/or treatment efficacy. Second, using a higher dosage of materials increases the risk of toxicity. Therefore, developing multifunctional systems has a critical role in improving human health.

Multifunctional diagnostic and therapeutic incorporate several nanomaterials into one host material. This material must be compatible with a wide variety of functional molecules and/or nanoparticles. Silica nanoparticles are an excellent example for a host material because they demonstrate multi-functionality, biocompatibility, stability, and biodegradability.

1.4 Advantages of silica nanoparticles

Silica nanoparticles have many advantages for medicine. First, the chemistry is easily tuned to create nanomaterials with defined sizes, shapes, and surface properties[91]. The easily modifiable chemistry in silica is essential for optimal biocompatibility and biodistribution[28, 92]. Silica nanoparticles synthesis has a history spanning over 60 years. Monodispersed amorphous silica nanoparticles were first synthesized by Kolbe in 1956[93] and was then improved by Stöber and Fink in 1968[94]. Stöber's method tunes the size of silica nanoparticles from tens of nanometers to several micrometers in diameter by changing the ratio of catalyst and precursor. In the early 1990s, "Template"-guided synthesis methods for mesoporous silica nanoparticles (MSNs) were reported by scientists from Japan and the Mobil corporation[95–97]. Examples of tunable silica nanomaterials include solid spheres[93, 94], mesoporous particles[95–98], mesoporous hollow spheres[99, 100], rattle-typed spheres[101], foam-like nanoparticles[102], nanotubes[103], mesoporous red blood cell-shaped nanoparticles[31], etc. Figures 3A–H show examples of silica nanoparticles with different morphologies[31]. In addition, the surface of silica nanoparticles can be easily modified with functional molecules[104] including spacers for colloidal stability[105], antibodies for active targeting[106], fluorophores for imaging[107], magnetic nanoparticles[108] for manipulation or MRI, gating molecules to stimulate drug release[109], functional groups to tune surface charge[32], and therapeutic agents[110] (Figure 3I).

Silica nanoparticles may have good biocompatibility because they degrade to nontoxic silicic acid *in vivo*[111–113], and silicic acid is naturally found in many tissues and can be excreted from the body through urine[112]. However, the toxicity depends on their dosage[114], crystallinity[34, 114, 115], particle size[91, 116, 117], surface properties[116, 118], and administration route[119, 120]. Higher dosage increases the risk for toxicity. Crystal silica nanoparticles are toxic and cause silicosis[115]. But amorphous silica has been used as a food additive for decades because of its excellent biocompatibility[34, 114]. Smaller particles have been reported

to be less biocompatible than larger ones[91, 116, 117], possibly due to the increased specific surface area. However, this is still controversial[121]. Decreasing the surface hydroxyl groups increases the silica nanoparticles biocompatibility[118]. The size and surface properties of amorphous silica nanoparticles can easily be tuned to increase the biocompatibility. Nanoparticles administered orally have less immunotoxicity than intravenous, intraperitoneal, and subcutaneous route, but also lower bioavailability with less availability for the immune cells to interact with the nanoparticles[121].

Silica nanoparticles are intrinsically stable, and moreover their degradability and circulation time can be tuned[122–125]. Generally, silica nanoparticles carry drug in their mesopores and release the drug through diffusion. Therefore, stability is important to enable the silica nanoparticles to be retained in the body and release the drug. This stability also guarantees no drug leakage from capped porous silica nanoparticles that release drug as a function of external stimuli[124, 126]. Though silica nanoparticles are usually cleared by the human body within a short time, surface modifications such as PEGylation can prolong the circulation period of silica nanoparticles[127]. On the other hand, imaging contrast agents need to be quickly cleared to decrease background signal and prevent interference with future scans. In this case, increasing the pore size of silica nanoparticles and doping them with metal ions can accelerate their degradation to get a short circulation time[113, 125].

Finally, pure silica nanoparticles have intrinsic theranostic potentials stemming from high acoustic mismatch with most soft tissues. Also, silica nanoparticles can be customized to label cells and tissues and therefore increase their ultrasound contrast after transplantation[31, 68, 128, 129]. The therapeutic effects of silica nanoparticles result from their large surface area and porous structures. The large surface area provides plenty of conjugation sites or physical binding sites for therapeutic molecules[130–132], and the pores in the silica nanoparticles can physically hold and protect cargo[133–135].

In summary, silica nanoparticles are ideal for nanomedicine and biomaterials research due to their various morphologies, facile chemical modification, tunable pore size and porosity, biocompatibility, tunable stability and biodegradability, and theranostic potential.

2. Synthesis, modification, and integration of silica nanoparticles

2.1 Synthesis of silica nanoparticles

Silica nanoparticles can be prepared via bottom-up or top-down methods. Bottom-up synthesis usually involves catalyzed hydrolysis and condensation of silica sources[94, 98]. The top-down synthesis of silica nanoparticles includes electrochemical etching of silicon wafer and pyrolysis of quartz sand[118, 136].

Bottom-up synthesis is very common in laboratory research because it is simple, safe, and can make various morphologies. Bottom-up synthesis typically uses an aqueous or ethanol based solvent, and this method usually involves silica sources, catalysts, and templates. The most prevalent silica source is an alkoxide of silicon scuh as tetraethyl orthosilicate (TEOS). The alkoxide first hydrolyzes and produces silicate species and alcohol (Equation 1). The silicates then condense and form Si-O-Si linkages (Equation 2). In addition, organosilanes

such as aminopropyl-trimethoxysilane and mercaptopropyl-methoxysilane are usually used as co-precursors, which can introduce functional groups to the silica nanoparticles surface[1].

$$Si(OR)_4 + H_2O \rightarrow (RO)_3Si(OH) + ROH \quad \text{Equation 1}$$

$$(RO)_3Si(OH) + (HO)Si(OR)_3 \rightarrow (RO)_3Si - O - Si(OR)_3 + H_2O \quad \text{Equation 2}$$

R represents alkyl groups and is usually methyl or ethyl groups. The hydrolysis of silica sources can be catalyzed either by acids or bases. Under basic conditions, the polymerization and condensation of silicate species are reversible, which makes it easier to obtain homogenous silica products. On the contrary, highly acidic conditions lead to rapid hydrolysis and precipitation of silica particles. The production of silica nanoparticles can be accelerated by decreasing pH, but that often results in poly-disperse products[98]. Templates are used to generate porous structure in the silica nanoparticles. The most common templates are surfactants that form micelles in solvents and create mesopores that are smaller than 5 nm. This pore size is suitable for small molecule cargos. Larger pores are needed to load macromolecules and small nanoparticles such as quantum dots. To enlarge silica nanoparticles pores, polymers and pore expanding agents are normally used[137]. Interestingly, cells and organs can also be used as templates[138, 139].

Top-down methods are more hazardous to implement because they require highly corrosive hydrofluoric acid (electrochemical etching) or high temperatures (>1500°C, pyrolysis)[140]. Moreover, tuning silica nanoparticles morphology is difficult using top-down methods. For example, fumed silica nanoparticles prepared by pyrolysis are nonporous and range in size from 5 to 50 nm. These nanoparticles are commonly used as light abrasives in toothpaste or as anticaking agents and desiccants. On the contrary, the silica nanoparticles obtained by electrochemical etching have an irregular 2D porous structure. The direct products from electrochemical etching are porous silicon stand-free films. To create porous silica nanoparticles, the silicon films are broken down by sonication and then oxidized[136, 141].

2.2 Surface modification of silica nanoparticles

The surface of silica nanoparticles can be modified with polymer chains either chemically (by covalent bonding) or physically (by physisorption)[142]. Physical modification is usually reversible. It is not as common as chemical modification due to the instability of the non-covalent bond[143].

Subsequent chemical modification is enabled by the silanol and siloxane groups on the silica. The number and form of the silanol groups changes as a function of synthesis route[118]. Colloidal silica nanoparticles are almost completely hydroxylated, and all silanols have hydrogen bonds. Fumed silica nanoparticles have much lower silanol contents—only about half of the surface has silanols. Approximately 10% of the silanols on fumed silica nanoparticle surfaces are isolated. Heat treatment can decrease the silanol content on both types of silica nanoparticles.[118]

Silanol groups are the main reason underlying the facile modification of silica nanoparticles. These groups can react with abundant and commercially available silane reagents. Silanes then introduce other functional groups onto the surface of silica nanoparticles. The most frequently used silanes have amine or sulfur groups at the end of an alkylsilane along with various PEG-silanes. Amine or thiol-ended groups offer a facile linker chemistry with commonly used linking moieties such as N-hydroxysuccinide (NHS) functionalized molecules, isothiocyanates, maleimides, etc[106, 144]. Both of these functional groups can also be used to tune the surface charge of the silica nanoparticles[32, 145]. Alkylsilanes are used for hydrophobic surface treatment and to increase the echogenicity of silica nanoparticles[146]. PEG-silanes graft PEG onto silica nanoparticles, improve the particles stability in biological fluids, and prolong the *in vivo* circulation time[147, 148]. Table 2 presents the most frequently used silanes for nanoparticle surface modification and their functions.

2.3 Formulations/functions of silica in integrated nanoparticles

Silica mainly exists as a core, shell, or matrix for doping in integrated nanoparticles. Table 3 summarizes the major functions of silica as a function of its formulation in the nanoparticles along with relevant literature sources. The synthesis of nanoparticles with a silica core involves the preparation of silica nanoparticles followed by a multi-step modification[106, 158, 159]. The synthesis of the silica core is similar to the preparation of silica nanoparticles—mainly polymerization and condensation of silica sources[98].

Similarly, the core/silica shell structures are made via a multistep procedure[160]. Generally, the silica shell is formed by growing a layer of silica on the surfaces of other nanomaterials such as gold nanoparticles, gold nanorods, quantum dots, and iron oxide nanoparticles. The surfaces should have a significant chemical or electrostatic affinity for silica[161], otherwise the surfaces need to be activated. For example, the surfaces of gold nanomaterials have a weak has and therefore stabilizers are typically used on the surface of gold to prevent coagulation. Therefore, the gold surface is usually treated with MPTMS before coating with silica[162].

Doping functional ions, functional groups, and/or molecules into the silica matrix is another method to create multi-functional nanoparticles[163, 164]. There are two methods to dope silica nanoparticles. The first method is a one-pot sol-gel synthesis that mixes silica sources with a wide variety of organic dye molecules, metal ion chelators, or even iron oxide or quantum dots[164]. The other method is reverse microemulsion, which is suitable for doping hydrophobic organic dyes into silica nanoparticles[165–167]. This method involves creating a homogeneous mixture of water, oil, and surfactant molecules; the dye molecules often need to be modified to increase their affinity for silica[165].

One big challenge for the translation of hybrid silica nanoparticles is simplified synthetic steps that integrate both cargo and carrier. It is currently difficult to achieve one-pot synthesis whereby the cargo is loaded into the nanoparticles as they are being synthetized. This is due to the multiple components involved—especially when sensitive therapeutic/diagnostic molecules are added. Thus, post-synthetic loading remains common to retain the biological activity of the sensitive molecular cargo. However, this method is time-consuming

and inefficient, which is difficult to be used industrially. Future research efforts should design creative ways to solve this problem.

3. Integrated silica nanoparticles in nanomedicine

3.1 Theranostic and multimodal imageable silica nanoparticles

Theranostic and multimodal imageable nanoparticles are nanoparticles that act as both diagnostic and therapeutic agents. Theranostic nanoparticles are valuable tools for identifying and selecting patients followed by treating selected patients positively. Multimodal nanoparticle contrast agents combine the advantages of different imaging modalities.

In this context, a variety of diagnostic information can be obtained depending on the particle design. For example, theranostic medicines can provide insights into the availability of a molecular target in the tissue, the vascular permeability and retention of the molecule, the drug release from the particle, and the response of the target tissue[178].

Nevertheless, the silica components in these integrated systems play various important roles in stabilizing and protecting the core nanoparticles or dopants. They offer multiple chemical modification methods and serve as a therapeutic reservoir to achieve target delivery and/or controlling release. For example, coupling fluorophores into silica nanoparticles can diminish the effect of fluorophore photobleaching. Peng et al. developed intracellular pH sensitive nanoparticles that can detect cellular pH from pH 4–7[144]. These nanoparticles are silica nanoparticles doped with two fluorophore sensors. Silica increases the stability and sensitivity of the fluorophores and allows for high quantification and measurement reversibility by diminishing photobleaching of the dyes.

Silica can also decrease the toxicity of nanoparticles that contain toxic components such as heavy metals. Doping functional elements such as lanthanide ions into silica is another useful strategy to make multifunctional nanoparticles. For example, gadolinium (Gd) is a commonly used MRI T1 contrast agent, but it is toxic due to its accumulation in tissues like brain, bone, and kidneys[179]. Silica nanoparticles doped with gadolinium not only improve the MRI contrast but also decrease the toxicity of Gd.

Rieter et al. added a paramagnetic monolayer of silylated Gd complex onto a luminescent $[Ru(2,2'\text{-bypyridine})_3]Cl_2$ core by a water-in-oil reverse microemulsion method[176]. This nanoparticle offers fluorescent and MRI signals due to the $[Ru(2,2'\text{-bypyridine})_3]Cl_2$ core and the Gd in the silica shell. The silica is also conjugated with diethylenetriaminetetraacetate (DTTA), which provides seven binding sites for Gd^{3+} ions to minimize the toxicity of nanoparticles owing to the leaching of Gd^{3+} centers. The nanoparticle is sufficiently small (<50 nm) to be endocytosed by monocyte cells and allows multimodal *in vitro* imaging of the cells. The authors are using this nanoparticle as target-specific contrast agents for optical and magnetic resonance (MR) imaging of rheumatoid arthritis in mice[176].

Our group previously designed a multimodal silica nanoparticle which has a fluorescent, ultrasound, and MRI signal[177]. The ultrasound contrast can increase the contrast of the stem cells and guide the injection of stem cells, and the MRI signal is proportional to the cell numbers, which can be used to track the cell numbers after injection. The nanoparticle was prepared based on the Stöber method including fluorescein isothiocyanate (FITC)-conjugated organosilanes with TEOS; $GdCl_3$ was used for Gd doping (Figure 4A). Silica produces ultrasound contrast because it has a high acoustic impedance mismatch with cells and soft tissues. Silica reflects more ultrasound, and thus the silica materials have more ultrasound signal than soft tissues in ultrasound images. The size of these nanoparticles can be tuned, and the ultrasound contrast of these nanoparticles is size dependent (Figure 4B–D). This nanoparticle is used to label and track stem cells to improve stem cell therapeutic efficacy.

Later work developed a theranostic system using this nanoparticle by introducing pores into the silica nanoparticle[113]. The nanoparticles retain the multimodal imaging signals–ultrasound, MRI, and fluorescence (Figure 5A–E). Sectioning transmission electron microscopy (TEM) images show these nanoparticles are located in the cytoplasm of the cell (Figure 5F–H). Moreover, the pores are used to load a prosurvival agent for stem cells and slowly release the insulin-like growth factor (IGF) inside cells (Figure 6A, B). This system increases cell survival up to 40% ($p<0.05$) versus unlabeled cells under *in vitro* serum-free culture conditions (Figure 6C).

Sweeney *et al.* used a similar silica nanoparticle doped with gadolinium oxide and conjugated with tetramethylrhodamine-isothiocyanate (TRITC) to improve real-time monitoring and staging of mouse bladder cancer models[180]. They injected murine flanks with MB49 cancer cells, and then injected silica nanoparticles to examine differences in MRI signal between tumors and bladder epithelium. The integrated silica nanoparticles enhanced both T1 and T2 weighted MRI signals in the tumors, allowing detailed *in vivo* evaluations (Figure 7). The localization of particles helped delineate the tumor's edges, which are usually difficult to detect. This system can potentially be used for theranostic purposes, as therapeutic carriers for anticancer agents, and diagnostic tools for tumor visualization.

Lin et al. developed a theranostic targeting mesoporous silica nanoparticle with multiple imaging modalities by doping and surface conjugation[181]. The nanoparticles are doped with europium (Eu) and Gd ions. These ions introduce fluorescence and magnetism to the mesoporous structure, and thus the nanoparticles can be used as a fluorescent tool. The MRI indicates the location and size of the tumor. The doped nanoparticle is then conjugated with the anticancer drug camptothecin (CPT) by disulfide bonds. This disulfide bond can be cleaved by a high concentration of intracellular glutathione for intracellular controlled release. Moreover, the surface of the nanoparticle is modified with folic acid, which can be used to target most human cancer cells. *In vitro* and *in vivo* studies show that these integrated silica nanoparticles can target, image, and destroy the tumors in mice.

Silica is also highly useful for assistance in functionalizing nanoparticles. Fluorescent and radio-opaque nanoparticles can be used for CT, MRI, and diffuse optical tomography[171].

They have a silica core that is doped with tris(2,2′-bipyridyl) dichlororuthenium(II) hexahydrate. The core is surrounded by a layer of n-(trimethoxysilyl-propyl)ethyldiamine tri-acetic acid trisodium salt that traps paramagnetic Gd^{3+} ions. Finally, the particles are wrapped by an additional silica shell layer containing amine groups on the surface that can be used for functionalization. This multimodal (optical, radiology, CT, and MRI) contrast agent can help in the preoperative diagnosis and in the intraoperative surgical resection of tumors or other surgical lesions[171].

Mesoporous silica-coated MnO nanoparticles also show great potential as MRI contrast agents for cell tracking[50]. These nanoparticles have a MnO/SiO_2 core shell structure, and the nanoparticles are named as $HMnO@mSiO_2$ nanoparticles where the symbol @ usually means inside. (Figure 8A, B). The innate r_1 relaxivity of MnO provides the MRI signal of the nanoparticle (Figure 8C, D). The silica increases the biocompatibility of MnO core. This nanoparticle can label MSCs *in vivo* and shows intense signals (Figure 8E, F). Moreover, the MRI signal can be detectable 14 days after the injection (Figure 8F).

The MnO/SiO_2 core shell structure can also be used for a theranostic and multimodal imaging system. Choi et al. embedded MnO/SiO_2 core/shell nanoparticles into porous poly(propylene fumarate) (PPF) scaffolds and used the MRI signal change to monitor the release of nanoparticles from the PPF scaffold surface. The anti-cancer drug doxorubicin (DOX) was loaded on the surface of the MnO/SiO_2 NPs by electrostatic interaction between the drug with the negatively charged porous silica surface[182]. Additionally, the porous silica shell can also enhance the water-dispersibility of the core and minimize the leakage of the core ions. Moreover, silica shell prevents the aggregation between MnO nanocores and therefore increases the dispersity of MnO nanocores.

Monaco et al. synthesized a core-shell $Fe_3O_4@SiO_2@Au$ nanosystem coated with 11-(4-mercaptobenzamido) undecanoate, poly(lactic-co-glycolic acid)-b-PEG-NH_2, and folic acid[183]. This nanosystem provides *in vivo* targeting capabilities and MRI-PA dual imaging signals. The combination of MRI and PAI offer mutual benefits—it overcame the depth and resolution limits of PAI and the temporal resolution of MRI. The MRI signal is produced by iron oxide while the PA signal is produced by the gold shell. The multilayer nanoparticles are then embedded in the so-called polymeric micelles to improve their biocompatibility[183]. The researchers then conjugated folic acid on the polymeric micelle surface to get a water-soluble nanocarrier that actively targets folate receptors that are often overexpressed in solid tumors. Their final system is highly biocompatible and can be manipulated to build other targetable nanostructures.

Mesoporous silica shells can also improve the performance of gold nanorods (AuNRs) in biomedical applications. AuNRs show great potential in multiple imaging modalities and therapies including CT, PA, PDT, and PTT. However, AuNRs have a low drug loading capacity and suffer from clustering, aggregation, and shape deformation. Zhang et al. fabricated a mesoporous silica shell coated AuNRs and loaded doxorubicin to the nanoparticle. These particles enable imaging, chemotherapeutics, and hyperthermia within a single nanoparticle platform for cancer treatments (Figure 8A)[184]. The silica forms a protective layer outside the AuNRs and prevents them from aggregation (Figure 8B, C). The

silica-coated nanorod showed stable surface plasmon resonance (Figure 8D). In addition, the release of doxorubicin from the nanoparticle can control the pH and near infra-red laser (Figure 8E). Moreover, the system can kill cancer cells by photothermal therapy. These properties make this nanoplatform a potential candidate for new therapeutic modalities such as image-guided drug delivery, hyperthermia, and combination therapy.

Kircher et. al. synthesized novel nanoparticles for MRI, photoacoustic, and Raman imaging in brain tumors[185]. These triple-modality contrast agents are used to delineat detailed brain tumor margins to remove more tumor tissue. These contrast agents are created with a 60-nm gold core, a Raman-active layer, a silica shell, and a gadolinium coating (Figure 9A, B). These nanoparticles are highly sensitive and detectable in the picomolar range for all three modalities (Figure 9C–E). In addition, it was shown that particles injected intravenously accumulated within the brain tumor but not in the adjacent healthy tissue (Figure 10), which allows for a noninvasive brain tumor delineation. This nanoparticle-based triple-modality contrast agent offers more accurate brain tumor imaging and resection.

Other than the functions mentioned above, Chen et al. also found that the silica shell can amplify the photoacoustic intensity of gold nanorods[172]. The group studied the relationship between photoacoustic signals and heat transfer properties in silica coated AuNRs. They found that the additional silica layer acted as a signal amplifier by reducing interfacial heat resistance between gold and a range of solvents (Figure 11). The addition of a silica layer 0-20 nm thick increased photoacoustic signal by up to 3-fold, peaking at 20 nm thickness. The addition of a silica layer to AuNRs appears to be a beneficial way to increase their utility as contrast agents for PAI.

3.2 Monitoring the release of therapeutic molecules

The real-time monitoring capabilities of molecules can provide an abundance of physiological and pathological information of the patients. Theranostic devices with integrated real-time monitoring abilities are emerging and offer more feedback on treatment. Integrated silica nanoparticles also show great potential in the field for real-time monitoring of molecules.

The silica component is an ideal cargo carrier. In 2005, Gruenhagen et al. monitored adenosine triphosphate (ATP) release from MCM-41 silica nanoparticles[186]. ATP was used as a model cargo and the release mechanism was studied through the use of ATP-activated luciferase, which produces bioluminescent signal with ATP exposure. Due to the capability of real-time monitoring for cargos during release, the authors found the release kinetics of encapsulated molecules can be controlled by changing the capping molecules.

Lai et al. (2013) reported a versatile fluorescence resonance energy transfer (FRET)-based drug delivery system[110]. These nanosystems consist of a coumarin-labeled cysteine tethered mesoporous silica nanoparticles as the drug carrier and a FITC-β-cyclodextrin (CD) as redox-responsive molecular gate blocking the pores. A FRET donor-acceptor pair of coumarin and FITC was integrated within the pore-unlocking event (Figure 12A). The presence of glutathione (GSH) in the environment of the particle provokes a redox response, unblocking the particle’s pores and releasing the encapsulated drugs. The extent of drug-

release can be controlled by the ratio of FITC-β-CD to GSH and monitored by pathological cell viability and FRET signals (Figure 12B).

Lai et al. developed a polypeptide-wrapped mesoporous silica coated multicolor up-conversion nanoparticle (UCNP@MSN) as a drug delivery system. This is advantageous because the drug release can be monitored in real-time[187]. They functionalized the system with zinc-dipicolylamine analogue (TDPA-Zn^{2+}) and wrapped it with polypeptides to entrap the loaded drug–DOX. The TDPA-Zn^{2+} and polypeptide layer caused DOX to quench the ultraviolet (UV) emission upconverted from incoming NIR by the upconversion nanoparticles. ATP displaced the peptides because it has a higher binding affinity with TDPA-Zn^{2+}. When ATP displaced the peptides, DOX was released through the open pores of the particles (Figure 13). The release can then be monitored through ratiometric changes in luminescence resonance energy transfer (LRET). The authors also showed that this system could be further functionalized with receptors like folic acids to distinguish different diseases.

Liu et al. synthesized an NIR-triggered nanosensor that monitors drug-release by using upconverted luminescence and MRI simultaneously[188]. The nanosensor is composed of UCNPs surrounded by a mesoporous silica shell as well as doxorubicin and azobenzene to create a FRET donor-acceptor pair with UCNP (Figure 14). They found that under NIR exposure, drugs loaded into the particles were released, which led to a steady increase in MRI and upconverted luminescence signals. DOX quenched the upconverted emission from UCNPs, and its release increased the upconverted luminescence signal intensity. The loaded drug also made it less likely for water molecules to bond with Gd^{3+} ions. When DOX was released, water from the surrounding environment diffused into the particle and interacted with Gd^{3+}. This increased the T1 MRI signal intensity.

The silica component can also act as fixative for small molecules to offer contrast for monitored drugs. Wang et al. conjugated Stöber silica nanoparticles with methylene blue to monitor the blood concentration of heparin in real time[32]. Methylene blue is an FDA approved dye and it shows thermal expansion when it absorbs infrared light, which is also known as photoacoustic signal. The authors showed that heparin could increase the photoacoustic signal of methylene blue, and moreover, the signal increase is proportional to the concentration of heparin within the clinical dosage range. Silica nanoparticles were used to immobilize the methylene blue and prevent this dye from diffusing into the circulation (Figure 15A). Silica adsorbs methylene blue through electrostatic forces, and the surface charge of the silica nanoparticles affects the sensitivity of detection. Thiol modified silica nanoparticles are more sensitive than non-modified ones (Figure 15B, C). PAI is based on ultrasound imaging. PAI inherits the real-time imaging performance and the signal is stable over time (Figure 15D). Therefore, this method can monitor the heparin concentration changes without waiting for long time. This system can also detect low molecular weight heparin, which is not detectable by the conventional method—activated partial thromboplastin time (aPTT).

Though the real-time monitoring capabilities of molecules can provide abundant of physiological and pathological information of the patients as well as feedback for

treatments, the development of such devices is still in its nascent stage because of the limitations of real-time imaging modalities. Therefore, more efforts are needed for real-time imaging modalities.

4. Conclusions and prospectives

Silica is critical for integrated nanoparticles and offers great potential in theranostic, multimodal imaging, and real-time monitoring for molecules. Silica nanoparticles are easily made and tuned to various morphologies. They also show great biocompatibility and tunable degradability. Silica nanoparticles themselves can be used for drug delivery and ultrasound imaging contrast agents. Moreover, silica nanoparticles can be easily combined with other inorganic and/or organic components, which offers more features. Integrated silica-based nanoparticles can be used in nuclear imaging, MRI, radiography, optical imaging, ultrasound imaging, and magnetic particle imaging. The integrated particles can also be used in target delivery, controlled release, radiation therapy, hyperthermia therapy, photodynamic therapy, and immunotherapy. Extensive research has shown the great potential of integrated silica nanoparticles in theranostic and multimodal imaging.

Despite the huge number of studies on silica-based integrated nanoparticles for applications in bio-imaging and drug delivery, they have not made a significant impact in the clinic yet. The only silica-based integrated nanoparticle close to FDA approval are C-dots, which exhibit positron emission tomography (PET) and optical dual-modality imaging[189]. More studies are needed to improve their colloidal stability, optimize biodistribution, and customize biodegradation to promote the translation of these nanomedicines. Moreover, similar to all the other nanomedicine systems, increasing the targetability of integrated silica nanoparticles is critical to their translation with respect to manufacturing, cost, toxicity, and imaging and therapeutic efficacy—targetability of nanoparticles affects the actual drug dose at the desired location[190].

We have summarized recent work that used integrated silica nanoparticles to monitor biomolecules. However, most of the systems are based on fluorescence, which is limited for *in vivo* and clinical study because of poor penetration depth of light. Therefore, developing new real-time imaging modalities with high penetration depth is necessary. Photoacoustic imaging is an emerging technique with both real-time capability and increased penetration depth[191]. However, the field is still premature due to the lack of designs for combining photoacoustic contrast agents with other functional materials. We expect that more integrated nano-designs will be studied to offer theranostic systems that also provide real-time feedback *in vivo*.

Acknowledgments

The authors would like to the National Institutes of Health grants R00 HL117048 and DP2 HL137187. We also acknowledge J. Lemaster for the help on the revision.

References

1. Xie J, Lee S, Chen X. Advanced drug delivery reviews. 2010; 62(11):1064–1079. [PubMed: 20691229]

2. Chen F, Zhao E, Kim T, Wang JX, Hableel G, Reardon PJT, Ananthakrishna SJ, Wang TY, Arconada-Alvarez S, Knowles JC, Jokerst JV. ACS Appl Mater Interfaces. 2017; 9(18):15566–15576. [PubMed: 28422482]
3. Liu Z, Tabakman S, Welsher K, Dai H. Nano Res. 2009; 2(2):85–120. [PubMed: 20174481]
4. Kostarelos K, Lacerda L, Pastorin G, Wu W, Sebastien Wieckowski, Luangsivilay J, Godefroy S, Pantarotto D, Briand J-P, Muller S, Prato M, Bianco A. Nat Nano. 2007; 2(2):108–113.
5. Yang S-T, Guo W, Lin Y, Deng X-Y, Wang H-F, Sun H-F, Liu Y-F, Wang X, Wang W, Chen M, Huang Y-P, Sun YP. The Journal of Physical Chemistry C. 2007; 111(48):17761–17764.
6. Lu F, Gu L, Meziani MJ, Wang X, Luo PG, Veca LM, Cao L, Sun YP. Advanced Materials. 2009; 21(2):139–152.
7. Mao HY, Laurent S, Chen W, Akhavan O, Imani M, Ashkarran AA, Mahmoudi M. Chem Rev. 2013; 113(5):3407–3424. [PubMed: 23452512]
8. He Q, Kiesewetter DO, Qu Y, Fu X, Fan J, Huang P, Liu Y, Zhu G, Liu Y, Qian Z, Chen X. Advanced Materials. 2015; 27(42):6741–6746. [PubMed: 26401893]
9. Feng L, Liu Z. Nanomedicine. 2011; 6(2):317–324. [PubMed: 21385134]
10. Zhang Y, Petibone D, Xu Y, Mahmood M, Karmakar A, Casciano D, Ali S, Biris AS. Drug metabolism reviews. 2014; 46(2):232–246. [PubMed: 24506522]
11. Huang SK, Stauffer PR, Hong KL, Guo JWH, Phillips TL, Huang A, Papahadjopoulos D. Cancer Res. 1994; 54(8):2186–2191. [PubMed: 8174126]
12. Kong G, Anyarambhatla G, Petros WP, Braun RD, Colvin OM, Needham D, Dewhirst MW. Cancer Res. 2000; 60(24):6950–6957. [PubMed: 11156395]
13. Torchilin VP. Nat Rev Drug Discov. 2005; 4(2):145–160. [PubMed: 15688077]
14. Weng KC, Noble CO, Papahadjopoulos-Sternberg B, Chen FF, Drummond DC, Kirpotin DB, Wang DH, Hom YK, Hann B, Park JW. Nano Lett. 2008; 8(9):2851–2857. [PubMed: 18712930]
15. Kukowska-Latallo JF, Bielinska AU, Johnson J, Spindler R, Tomalia DA, Baker JR. Proceedings of the National Academy of Sciences. 1996; 93(10):4897–4902.
16. Gillies ER, Fréchet JMJ. Drug Discov Today. 2005; 10(1):35–43. 17. [PubMed: 15676297]
17. Svenson S, Tomalia DA. Advanced Drug Delivery Reviews. 2012; 64(Supplement):102–115.
18. Lee CC, MacKay JA, Frechet JMJ, Szoka FC. Nat Biotech. 2005; 23(12):1517–1526.
19. Tomalia DA, Naylor AM, Goddard WA. Angewandte Chemie International Edition in English. 1990; 29(2):138–175.
20. Alexis F, Pridgen E, Molnar LK, Farokhzad OC. Molecular Pharmaceutics. 2008; 5(4):505–515. [PubMed: 18672949]
21. Pinto Reis C, Neufeld RJ, Ribeiro AJ, Veiga F. Nanomedicine: Nanotechnology, Biology and Medicine. 2006; 2(1):8–21.
22. Kumari A, Yadav SK, Yadav SC. Colloids and Surfaces B: Biointerfaces. 2010; 75(1):1–18. [PubMed: 19782542]
23. Owens DE III, Peppas NA. International Journal of Pharmaceutics. 2006; 307(1):93–102. [PubMed: 16303268]
24. Soppimath KS, Aminabhavi TM, Kulkarni AR, Rudzinski WE. Journal of Controlled Release. 2001; 70(1–2):1–20. [PubMed: 11166403]
25. Galaev IY, Mattiasson B. Trends in Biotechnology. 1999; 17(8):335–340. [PubMed: 10407406]
26. Jokerst JV, Van de Sompel D, Bohndiek SE, Gambhir SS. Photoacoustics. 2014; 2(3):119–127. [PubMed: 25225633]
27. Anglin EJ, Cheng L, Freeman WR, Sailor MJ. Advanced Drug Delivery Reviews. 2008; 60(11): 1266–1277. [PubMed: 18508154]
28. Tang F, Li L, Chen D. Advanced Materials. 2012; 24(12):1504–1534. [PubMed: 22378538]
29. Li Z, Barnes JC, Bosoy A, Stoddart JF, Zink JI. Chemical Society Reviews. 2012; 41(7):2590–2605. [PubMed: 22216418]
30. Slowing II, Vivero-Escoto JL, Wu CW, Lin VSY. Advanced Drug Delivery Reviews. 2008; 60(11): 1278–1288. [PubMed: 18514969]

31. Chen F, Ma M, Wang J, Wang F, Chern SX, Zhao ER, Jhunjhunwala A, Darmadi S, Chen H, Jokerst JV. Nanoscale. 2017; 9(1):402–411. [PubMed: 27924340]
32. Wang JX, Chen F, Arconada-Alvarez SJ, Hartanto J, Yap LP, Park R, Wang F, Vorobyova I, Dagliyan G, Conti PS, Jokerst JV. Nano Letters. 2016; 16(10):6265–6271.
33. Slowing I, Trewyn BG, Lin VSY. Journal of the American Chemical Society. 2006; 128(46): 14792–14793. [PubMed: 17105274]
34. Lu J, Liong M, Li Z, Zink JI, Tamanoi F. Small. 2010; 6(16):1794–1805. [PubMed: 20623530]
35. Foroutan F, Jokerst JV, Gambhir SS, Vermesh O, Kim HW, Knowles JC. ACS Nano. 2015; 9(2): 1868–1877. [PubMed: 25625373]
36. Bagalkot V, Zhang L, Levy-Nissenbaum E, Jon S, Kantoff PW, Langer R, Farokhzad OC. Nano Letters. 2007; 7(10):3065–3070. [PubMed: 17854227]
37. Liu WH, Choi HS, Zimmer JP, Tanaka E, Frangioni JV, Bawendi M. Journal of the American Chemical Society. 2007; 129(47):14530–+. [PubMed: 17983223]
38. Liu W, Howarth M, Greytak AB, Zheng Y, Nocera DG, Ting AY, Bawendi MG. Journal of the American Chemical Society. 2008; 130(4):1274–1284. [PubMed: 18177042]
39. Smith AM, Duan H, Mohs AM, Nie S. Adv Drug Deliv Rev. 2008; 60(11):1226–1240. [PubMed: 18495291]
40. Wang L, Yan R, Huo Z, Wang L, Zeng J, Bao J, Wang X, Peng Q, Li Y. Angewandte Chemie International Edition. 2005; 44(37):6054–6057. [PubMed: 16118828]
41. Chen G, Qiu H, Prasad PN, Chen X. Chem Rev. 2014; 114(10):5161–5214. [PubMed: 24605868]
42. Sun LD, Wang YF, Yan CH. Accounts Of Chemical Research. 2014; 47(4):1001–1009. [PubMed: 24422455]
43. Lv R, Yang P, Hu B, Xu J, Shang W, Tian J. ACS Nano. 2017; 11(1):1064–1072. [PubMed: 27960062]
44. Muhr V, Wilhelm S, Hirsch T, Wolfbeis OS. Accounts Of Chemical Research. 2014; 47(12):3481–3493. [PubMed: 25347798]
45. Fang C, Zhang M. Journal of Materials Chemistry. 2009; 19(35):6258–6266. [PubMed: 20593005]
46. Gupta AK, Gupta M. Biomaterials. 2005; 26(18):3995–4021. [PubMed: 15626447]
47. Laurent S, Forge D, Port M, Roch A, Robic C, Vander Elst L, Muller RN. Chem Rev. 2008; 108(6):2064–2110. [PubMed: 18543879]
48. Bulte JWM, Kraitchman DL. NMR in Biomedicine. 2004; 17(7):484–499. [PubMed: 15526347]
49. Tartaj P, del Puerto Morales M, Veintemillas-Verdaguer S, González-Carreño T, Serna CJ. Journal of Physics D: Applied Physics. 2003; 36(13):R182.
50. Zhen Z, Xie J. Theranostics. 2012; 2(1):45–54. [PubMed: 22272218]
51. Rasmussen JW, Martinez E, Louka P, Wingett DG. Expert opinion on drug delivery. 2010; 7(9): 1063–1077. [PubMed: 20716019]
52. LaVan DA, McGuire T, Langer R. Nature Biotechnology. 2003; 21:1184.
53. Kim T, Lemaster JE, Chen F, Li J, Jokerst JV. ACS Nano. 2017; 11(9):9022–9032. [PubMed: 28759195]
54. Jain PK, Huang X, El-Sayed IH, El-Sayed MA. Accounts Of Chemical Research. 2008; 41(12): 1578–1586. [PubMed: 18447366]
55. Hu M, Chen J, Li ZY, Au L, Hartland GV, Li X, Marquez M, Xia Y. Chemical Society Reviews. 2006; 35(11):1084–1094. [PubMed: 17057837]
56. Ghosh P, Han G, De M, Kim CK, Rotello VM. Advanced Drug Delivery Reviews. 2008; 60(11): 1307–1315. [PubMed: 18555555]
57. El-Sayed IH, Huang X, El-Sayed MA. Nano Letters. 2005; 5(5):829–834. [PubMed: 15884879]
58. Daniel MC, Astruc D. Chem Rev. 2004; 104(1):293–346. [PubMed: 14719978]
59. Chen Y, Wang M, Mao C. Angewandte Chemie International Edition. 2004; 43(27):3554–3557. [PubMed: 15293243]
60. Zheng J, Birktoft JJ, Chen Y, Wang T, Sha R, Constantinou PE, Ginell SL, Mao C, Seeman NC. Nature. 2009; 461(7260):74–77. [PubMed: 19727196]
61. Roy K, Mao HQ, Huang SK, Leong KW. Nat Med. 1999; 5(4):387–391. [PubMed: 10202926]

62. Vijayanathan V, Thomas T, Thomas TJ. Biochemistry. 2002; 41(48):14085–14094. [PubMed: 12450371]
63. Thakor AS, Jokerst JV, Ghanouni P, Campbell JL, Mittra E, Gambhir SS. Journal of Nuclear Medicine. 2016; 57(12):1833–1837. [PubMed: 27738007]
64. McNeil SE. Journal of Leukocyte Biology. 2005; 78(3):585–594. [PubMed: 15923216]
65. McNeil SE. Wiley Interdisciplinary Reviews: Nanomedicine and Nanobiotechnology. 2009; 1(3): 264–271. [PubMed: 20049796]
66. Sun T, Zhang YS, Pang B, Hyun DC, Yang M, Xia Y. Angewandte Chemie International Edition. 2014; 53(46):12320–12364. [PubMed: 25294565]
67. Foroutan F, Jokerst JV, Gambhir SS, Vermesh O, Kim HW, Knowles JC. ACS Nano. 2015; 9(2): 1868–1877. [PubMed: 25625373]
68. Wang JX, Jokerst JV. Stem Cells Int. 2016
69. Nirmal M, Brus L. Accounts Of Chemical Research. 1999; 32(5):407–414.
70. He S, Johnson NJJ, Nguyen Huu VA, Cory E, Huang Y, Sah RL, Jokerst JV, Almutairi A. Nano Letters. 2017; 17(8):4873–4880. [PubMed: 28657755]
71. Zeng S, Baillargeat D, Ho HP, Yong KT. Chemical Society Reviews. 2014; 43(10):3426–3452. [PubMed: 24549396]
72. Jokerst JV, Cole AJ, Van de Sompel D, Gambhir SS. ACS Nano. 2012; 6(11):10366–77. [PubMed: 23101432]
73. Chen Z, Ma L, Liu Y, Chen C. Theranostics. 2012; 2(3):238. [PubMed: 22509193]
74. Zhang Y, Long M, Huang P, Yang H, Chang S, Hu Y, Tang A, Mao L. Scientific reports. 2016; 6:33335. [PubMed: 27616592]
75. Yang H, Mao H, Wan Z, Zhu A, Guo M, Li Y, Li X, Wan J, Yang X, Shuai X. Biomaterials. 2013; 34(36):9124–9133. [PubMed: 24008037]
76. Lemaster JE, Jokerst JV. Wiley Interdisciplinary Reviews: Nanomedicine and Nanobiotechnology. 2017; 9(1):e1404–n/a.
77. Ruan Q, Zhu Y, Li F, Xiao J, Zeng Y, Xu F. Investigation of layer-by-layer assembled heparin and chitosan multilayer films via electrochemical spectroscopy. 2009; 333:725–33.
78. Huang X, Jain PK, El-Sayed IH, El-Sayed MA. Nanomedicine. 2007; 2(5):681–693. [PubMed: 17976030]
79. Barua S, Mitragotri S. Nano Today. 2014; 9(2):223–243. [PubMed: 25132862]
80. McNeil SE. Wiley interdisciplinary reviews. Nanomedicine and nanobiotechnology. 2009; 1(3): 264–71. [PubMed: 20049796]
81. Kempen PJ, Kircher MF, de la Zerda A, Zavaleta CL, Jokerst JV, Mellinghoff IK, Gambhir SS, Sinclair R. Micron (Oxford, England: 1993). 2015; 68:70–76.
82. Jokerst JV, Chen Z, Xu L, Nolley R, Chang E, Mitchell B, Brooks JD, Gambhir SS. PLoS One. 2015; 10(9):e0139484. [PubMed: 26421725]
83. Alivisatos AP, Andrews AM, Boyden ES, Chun M, Church GM, Deisseroth K, Donoghue JP, Fraser SE, Lippincott-Schwartz J, Looger LL, Masmanidis S, McEuen PL, Nurmikko AV, Park H, Peterka DS, Reid C, Roukes ML, Scherer A, Schnitzer M, Sejnowski TJ, Shepard KL, Tsao D, Turrigiano G, Weiss PS, Xu C, Yuste R, Zhuang X. ACS Nano. 2013; 7(3):1850–66. [PubMed: 23514423]
84. Li M, Yang XJ, Ren JS, Qu KG, Qu XG. Advanced Materials. 2012; 24(13):1722–1728. [PubMed: 22407491]
85. Suarez S, Almutairi A, Christman KL. Biomaterials Science. 2015; 3(4):564–580. [PubMed: 26146548]
86. Mulder WJM, Fayad ZA. Arteriosclerosis, Thrombosis, and Vascular Biology. 2008; 28(5):801–802.
87. Tai JH, Foster P, Rosales A, Feng B, Hasilo C, Martinez V, Ramadan S, Snir J, Melling CWJ, Dhanvantari S, Rutt B, White DJG. Diabetes. 2006; 55(11):2931–2938. [PubMed: 17065328]
88. Ma Z, Lim TM, Lim LY. International Journal of Pharmaceutics. 2005; 293(1–2):271–280. [PubMed: 15778065]

89. Ho IT, Sessler JL, Gambhir SS, Jokerst JV. Analyst. 2015; 140(11):3731–3737. [PubMed: 25854506]
90. Gibney, M. 2013.
91. Lin W, Huang Y-W, Zhou XD, Ma Y. Toxicol Appl Pharmacol. 2006; 217(3):252–259. [PubMed: 17112558]
92. Almeida JP, Chen AL, Foster A, Drezek R. Nanomedicine (London, England). 2011; 6(5):815–35.
93. Kolbe G. Das komplexchemische verhalten der kieselsäure. 1956
94. Stöber W, Fink A, Bohn E. J Colloid Interface Sci. 1968; 26(1):62–69.
95. Yanagisawa T, Shimizu T, Kuroda K, Kato C. Bulletin of the Chemical Society of Japan. 1990; 63(4):988–992.
96. Beck J, Vartuli J, Roth WJ, Leonowicz M, Kresge C, Schmitt K, Chu C, Olson DH, Sheppard E. Journal of the American Chemical Society. 1992; 114(27):10834–10843.
97. Kresge CT, L ME, Roth WJ, Vartuli JC, Beck JS. Nature Materials. 1992; 359:710–712.
98. Wan Y, Zhao DY. Chem Rev. 2007; 107(7):2821–2860. [PubMed: 17580976]
99. Zhang T, Ge J, Hu Y, Zhang Q, Aloni S, Yin Y. Angewandte Chemie International Edition. 2008; 47(31):5806–5811. [PubMed: 18574831]
100. Chen F, Hong H, Shi S, Goel S, Valdovinos HF, Hernandez R, Theuer CP, Barnhart TE, Cai W. Sci Rep. 2014; 4
101. Zhang K, Chen H, Guo X, Zhang D, Zheng Y, Zheng H, Shi J. Sci Rep. 2015; 5:8766–8776. [PubMed: 25739832]
102. Schmidt-Winkel P, Lukens WW, Zhao D, Yang P, Chmelka BF, Stucky GD. Journal of the American Chemical Society. 1999; 121(1):254–255.
103. Fan R, Wu Y, Li D, Yue M, Majumdar A, Yang P. Journal of the American Chemical Society. 2003; 125(18):5254–5255. [PubMed: 12720419]
104. Kumar R, Roy I, Ohulchanskyy TY, Goswami LN, Bonoiu AC, Bergey EJ, Tramposch KM, Maitra A, Prasad PN. ACS Nano. 2008; 2(3):449–456. [PubMed: 19206569]
105. Bagwe RP, Hilliard LR, Tan W. Langmuir. 2006; 22(9):4357–4362. [PubMed: 16618187]
106. Tsai CP, Chen CY, Hung Y, Chang FH, Mou CY. Journal of Materials Chemistry. 2009; 19(32): 5737–5743.
107. Yang H, Zhuang Y, Hu H, Du X, Zhang C, Shi X, Wu H, Yang S. Advanced Functional Materials. 2010; 20(11):1733–1741.
108. Lee JE, Lee N, Kim H, Kim J, Choi SH, Kim JH, Kim T, Song IC, Park SP, Moon WK, Hyeon T. Journal of the American Chemical Society. 2010; 132(2):552–557. [PubMed: 20017538]
109. Zhu Y, Fujiwara M. Angewandte Chemie International Edition. 2007; 46(13):2241–2244. [PubMed: 17295377]
110. Lai JP, Shah BP, Garfunkel E, Lee KB. Acs Nano. 2013; 7(3):2741–2750. [PubMed: 23445171]
111. Shen D, Yang J, Li X, Zhou L, Zhang R, Li W, Chen L, Wang R, Zhang F, Zhao D. Nano Letters. 2014; 14(2):923–932. [PubMed: 24467566]
112. Park J-H, Gu L, Maltzahn Gv, Ruoslahti E, Bhatia SN, Sailor M. J Nature Mater. 2009; 8:331–336.
113. Kempen PJ, Greasley S, Parker KA, Campbell JL, Chang HY, Jones JR, Sinclair R, Gambhir SS, Jokerst JV. Theranostics. 2015; 5(6):631–642. [PubMed: 25825602]
114. Liu T, Li L, Teng X, Huang X, Liu H, Chen D, Ren J, He J, Tang F. Biomaterials. 2011; 32(6): 1657–1668. [PubMed: 21093905]
115. Rimal B, Greenberg AK, Rom WN. Curr Opin Pulm Med. 2005; 11(2):169–73. [PubMed: 15699791]
116. Napierska D, Thomassen LCJ, Rabolli V, Liston D, Gonzalez L, Kirsch-Volders M, Martens JA, Hoet PH. Small. 2009; 5(7):846–853. [PubMed: 19288475]
117. Nishimori H, Kondoh M, Isoda K, Tsunoda S-I, Tsutsumi Y, Yagi K. European Journal of Pharmaceutics and Biopharmaceutics. 2009; 72(3):496–501. [PubMed: 19232391]

118. Zhang HY, Dunphy DR, Jiang XM, Meng H, Sun BB, Tarn D, Xue M, Wang X, Lin SJ, Ji ZX, Li RB, Garcia FL, Yang J, Kirk ML, Xia T, Zink JI, Nel A, Brinker CJ. Journal of the American Chemical Society. 2012; 134(38):15790–15804. [PubMed: 22924492]
119. Fu C, Liu T, Li L, Liu H, Chen D, Tang F. Biomaterials. 2013; 34(10):2565–2575. [PubMed: 23332175]
120. Mamaeva V, Sahlgren C, Lindén M. Advanced Drug Delivery Reviews. 2013; 65(5):689–702. [PubMed: 22921598]
121. Elsabahy M, Wooley KL. Chemical Society Reviews. 2013; 42(12):5552–5576. [PubMed: 23549679]
122. Cauda V, Schlossbauer A, Bein T. Microporous and Mesoporous Materials. 2010; 132(1–2):60–71.
123. Hao N, Liu H, Li L, Chen D, Li L, Tang F. J Nanosci Nanotechnol. 2012; 12(8):6346–54. [PubMed: 22962747]
124. Zhai W, He C, Wu L, Zhou Y, Chen H, Chang J, Zhang H. Journal of Biomedical Materials Research Part B: Applied Biomaterials. 2012; 100B(5):1397–1403.
125. Labbaf S, Tsigkou O, Müller KH, Stevens MM, Porter AE, Jones JR. Biomaterials. 2011; 32(4):1010–1018. [PubMed: 21071080]
126. Zhao Y, Vivero-Escoto JL, Slowing II, Trewyn BG, Lin VS. Expert opinion on drug delivery. 2010; 7(9):1013–29. [PubMed: 20716017]
127. Jokerst JV, Lobovkina T, Zare RN, Gambhir SS. Nanomedicine. 2011; 6(4):715–728. [PubMed: 21718180]
128. Hartanto, J., Jokerst, JV. Nanoparticles for Ultrasound-Guided Imaging of Cell Implantation. In: Bulte, JWM., Modo, MMJ., editors. Design and Applications of Nanoparticles in Biomedical Imaging. Springer International Publishing; Cham: 2017. p. 299-314.
129. Zhou Y, Han X, Jing X, Chen Y. Advanced healthcare materials. 2017; 6(18)
130. Ahn B, Park J, Singha K, Park H, Kim WJ. Journal of Materials Chemistry B. 2013; 1(22):2829–2836.
131. Zhang W, Shen J, Su H, Mu G, Sun JH, Tan CP, Liang XJ, Ji LN, Mao ZW. ACS Appl Mater Interfaces. 2016; 8(21):13332–13340. [PubMed: 27164222]
132. Min Y, Li J, Liu F, Yeow EKL, Xing B. Angewandte Chemie. 2014; 126(4):1030–1034.
133. Yilmaz MD, Xue M, Ambrogio MW, Buyukcakir O, Wu Y, Frasconi M, Chen X, Nassar MS, Stoddart JF, Zink JI. Nanoscale. 2014; 7(3):1067–72.
134. Li X, Zhou L, Wei Y, El-Toni AM, Zhang F, Zhao D. Journal of the American Chemical Society. 2014; 136(42):15086–15092. [PubMed: 25251874]
135. Khashab NM, Trabolsi A, Lau YA, Ambrogio MW, Friedman DC, Khatib HA, Zink JI, Stoddart JF. Eur J Org Chem. 2009; 2009(11):1669–1673.
136. Qin Z, Joo J, Gu L, Sailor MJ. Part Part Syst Charact. 2013
137. Zhao D, Feng J, Huo Q, Melosh N, Fredrickson GH, Chmelka BF, Stucky GD. Science. 1998; 279(5350):548–552. [PubMed: 9438845]
138. Kaehr B, Townson JL, Kalinich RM, Awad YH, Swartzentruber BS, Dunphy DR, Brinker CJ. Proceedings of the National Academy of Sciences. 2012; 109(43):17336–17341.
139. Lou YR, Kanninen L, Kaehr B, Townson JL, Niklander J, Harjumäki R, Brinker CJ, Yliperttula M. Scientific reports. 2015:5.
140. Garrett, P. Defoaming: theory and industrial applications. Vol. 45. CRC Press; 1992.
141. Anglin EJ, Cheng L, Freeman WR, Sailor MJ. Adv Drug Deliv Rev. 2008; 60(11):1266–77. [PubMed: 18508154]
142. Zhao B, Brittain WJ. Progress in Polymer Science. 2000; 25(5):677–710.
143. Belder GF, ten Brinke G, Hadziioannou G. Langmuir. 1997; 13(15):4102–4105.
144. Peng JF, He XX, Wang KM, Tan WH, Wang Y, Liu Y. ANAL BIOANAL CHEM. 2007; 388(3):645–654. [PubMed: 17440714]
145. Wang Y, Sun Y, Wang J, Yang Y, Li Y, Yuan Y, Liu C. ACS Appl Mater Interfaces. 2016; 8(27):17166–17175. [PubMed: 27314423]

146. Jin Q, Lin CY, Kang ST, Chang YC, Zheng H, Yang CM, Yeh CK. Ultrason Sonochem. 2017; 36:262–269. [PubMed: 28069209]
147. He Q, Zhang Z, Gao F, Li Y, Shi J. Small. 2011; 7(2):271–80. [PubMed: 21213393]
148. Cauda V, Argyo C, Bein T. Journal of Materials Chemistry. 2010; 20(39):8693–8699.
149. He XX, Wang KM, Tan WH, Liu B, Lin X, He CM, Li D, Huang SS, Li J. Journal of the American Chemical Society. 2003; 125(24):7168–7169. [PubMed: 12797777]
150. Tan WH, Wang KM, He XX, Zhao XJ, Drake T, Wang L, Bagwe RP. Med Res Rev. 2004; 24(5): 621–638. [PubMed: 15224383]
151. Shaffer TM, Harmsen S, Khwaja E, Kircher MF, Drain CM, Grimm J. Nano Letters. 2016; 16(9): 5601–5604. [PubMed: 27464258]
152. van Vlerken LE, Vyas TK, Amiji MM. Pharmaceutical Research. 2007; 24(8):1405–1414. [PubMed: 17393074]
153. Zhang X, Shi F, Niu J, Jiang YG, Wang ZQ. Journal of Materials Chemistry. 2008; 18(6):621–633.
154. Jin QF, Lin CY, Kang ST, Chang YC, Zheng HR, Yang CM, Yeh CK. Ultrasonics Sonochemistry. 2017; 36:262–269. [PubMed: 28069209]
155. Zhang P, Kong J. Talanta. 2015; 134(Supplement C):501–507. [PubMed: 25618700]
156. Popat A, Liu J, Lu GQM, Qiao SZ. Journal of Materials Chemistry. 2012; 22(22):11173–11178.
157. Agostini A, Mondragón L, Coll C, Aznar E, Marcos MD, Martínez-Máñez R, Sancenón F, Soto J, Pérez-Payá E, Amorós P. ChemistryOpen. 2012; 1(1):17–20. [PubMed: 24551487]
158. Chen F, Zhu Y. Microporous and Mesoporous Materials. 2012; 150(0):83–89.
159. Fu J, Zhao Y, Zhu Y, Chen F. Nanomaterials in Drug Delivery, Imaging, and Tissue Engineering. : 237–268.
160. Anderson BD, Wu WC, Tracy JB. Chemistry of Materials. 2016; 28(14):4945–4952.
161. Liz-Marzán LM, Giersig M, Mulvaney P. Langmuir. 1996; 12(18):4329–4335.
162. Liu N, Prall BS, Klimov VI. Journal of the American Chemical Society. 2006; 128(48):15362–15363. [PubMed: 17131988]
163. Pohaku Mitchell KK, Liberman A, Kummel AC, Trogler WC. Journal of the American Chemical Society. 2012; 134(34):13997–14003. [PubMed: 22871140]
164. Bae SW, Tan W, Hong JI. Chemical Communications. 2012; 48(17):2270–2282. [PubMed: 22258619]
165. Zhao X, Bagwe RP, Tan W. Advanced Materials. 2004; 16(2):173–176.
166. Wang L, Yang C, Tan W. Nano Letters. 2005; 5(1):37–43. [PubMed: 15792409]
167. Santra S, Wang KM, Tapec R, Tan WH. Journal of biomedical optics. 2001; 6(2):160–166. [PubMed: 11375725]
168. Monaco I, Arena F, Biffi S, Locatelli E, Bortot B, La Cava F, Marini GM, Severini GM, Terreno E, Comes Franchini M. Bioconjug Chem. 2017; 28(5):1382–1390. [PubMed: 28453929]
169. Popat A, Hartono SB, Stahr F, Liu J, Qiao SZ, Qing Lu G. Nanoscale. 2011; 3(7):2801–2818. [PubMed: 21547299]
170. Chen F, Hong H, Zhang Y, Valdovinos HF, Shi S, Kwon GS, Theuer CP, Barnhart TE, Cai W. ACS Nano. 2013; 7(10):9027–9039. [PubMed: 24083623]
171. Santra S, Bagwe RP, Dutta D, Stanley JT, Walter GA, Tan W, Moudgil BM, Mericle RA. Advanced Materials. 2005; 17(18):2165–2169.
172. Chen YS, Frey W, Kim S, Kruizinga P, Homan K, Emelianov S. Nano Letters. 2011; 11(2):348–354. [PubMed: 21244082]
173. Zhao W, Gu J, Zhang L, Chen H, Shi J. Journal of the American Chemical Society. 2005; 127(25):8916–8917. [PubMed: 15969545]
174. Wang H, Brandl DW, Nordlander P, Halas NJ. Accounts Of Chemical Research. 2007; 40(1):53–62. [PubMed: 17226945]
175. Zhang F, Braun GB, Shi Y, Zhang Y, Sun X, Reich NO, Zhao D, Stucky G. Journal of the American Chemical Society. 2010; 132(9):2850–2851. [PubMed: 20158187]

176. Rieter WJ, Kim JS, Taylor KML, An H, Lin W, Tarrant T, Lin W. Angewandte Chemie. 2007; 119(20):3754–3756.
177. Jokerst JV, Khademi C, Gambhir SS. Sci Transl Med. 2013; 5(177):177ra35.
178. Kiessling F, Mertens ME, Grimm J, Lammers T. Radiology. 2014; 273(1):10–28. [PubMed: 25247562]
179. Rogosnitzky M, Branch S. Biometals. 2016; 29:365–376. [PubMed: 27053146]
180. Sweeney SK, Luo Y, O'Donnell MA, Assouline J. Cancer Nanotechnology. 2016; 7:3. [PubMed: 27217840]
181. Chan M-H, Lin H-M. Biomaterials. 2015; 46:149–158. [PubMed: 25678124]
182. Choi J, Kim K, Kim T, Liu G, Bar-Shir A, Hyeon T, McMahon MT, Bulte JW, Fisher JP, Gilad AA. Journal of controlled release. 2011; 156(2):239–245. [PubMed: 21763735]
183. Monaco I, Arena F, Biffi S, Locatelli E, Bortot B, La Cava F, Marini GM, Severini GM, Terreno E, Comes Franchini M. Bioconjugate Chemistry. 2017; 28(5):1382–1390. [PubMed: 28453929]
184. Zhang Z, Wang L, Wang J, Jiang X, Li X, Hu Z, Ji Y, Wu X, Chen C. Advanced Materials. 2012; 24(11):1418–1423. [PubMed: 22318874]
185. Kircher MF, de la Zerda A, Jokerst JV, Zavaleta CL, Kempen PJ, Mittra E, Pitter K, Huang R, Campos C, Habte F, Sinclair R, Brennan CW, Mellinghoff IK, Holland EC, Gambhir SS. Nat Med. 2012; 18(5):829–834. [PubMed: 22504484]
186. Gruenhagen JA, Lai CY, Radu DR, Lin VSY, Yeung ES. Applied Spectroscopy. 2005; 59(4):424–431. [PubMed: 15901327]
187. Lai JP, Shah BR, Zhang YX, Yang LT, Lee KB. Acs Nano. 2015; 9(5):5234–5245. [PubMed: 25859611]
188. Liu JN, Bu JW, Bu WB, Zhang SJ, Pan LM, Fan WP, Chen F, Zhou LP, Peng WJ, Zhao KL, Du JL, Shi JL. Angewandte Chemie-International Edition. 2014; 53(18):4551–4555. [PubMed: 24668766]
189. Anselmo AC, Mitragotri S. The AAPS Journal. 2015; 17(5):1041–1054. [PubMed: 25956384]
190. Wilhelm S, Tavares AJ, Dai Q, Ohta S, Audet J, Dvorak HF, Chan WCW. Nature Reviews Materials. 2016; 1:16014.
191. Bohndiek SE, Sasportas LS, Machtaler S, Jokerst JV, Hori S, Gambhir SS. Journal of nuclear medicine: official publication, Society of Nuclear Medicine. 2015; 56(12):1942–7.

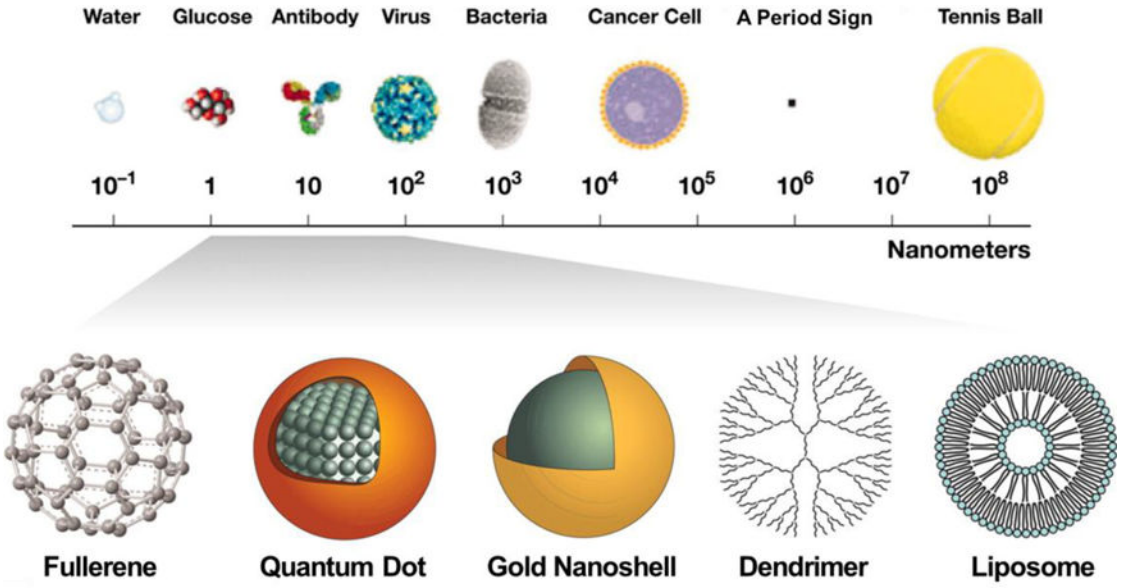

Figure 1.

The sizes of nanomaterials are comparable to biomolecules and organisms. (Adapted from reference[64]).

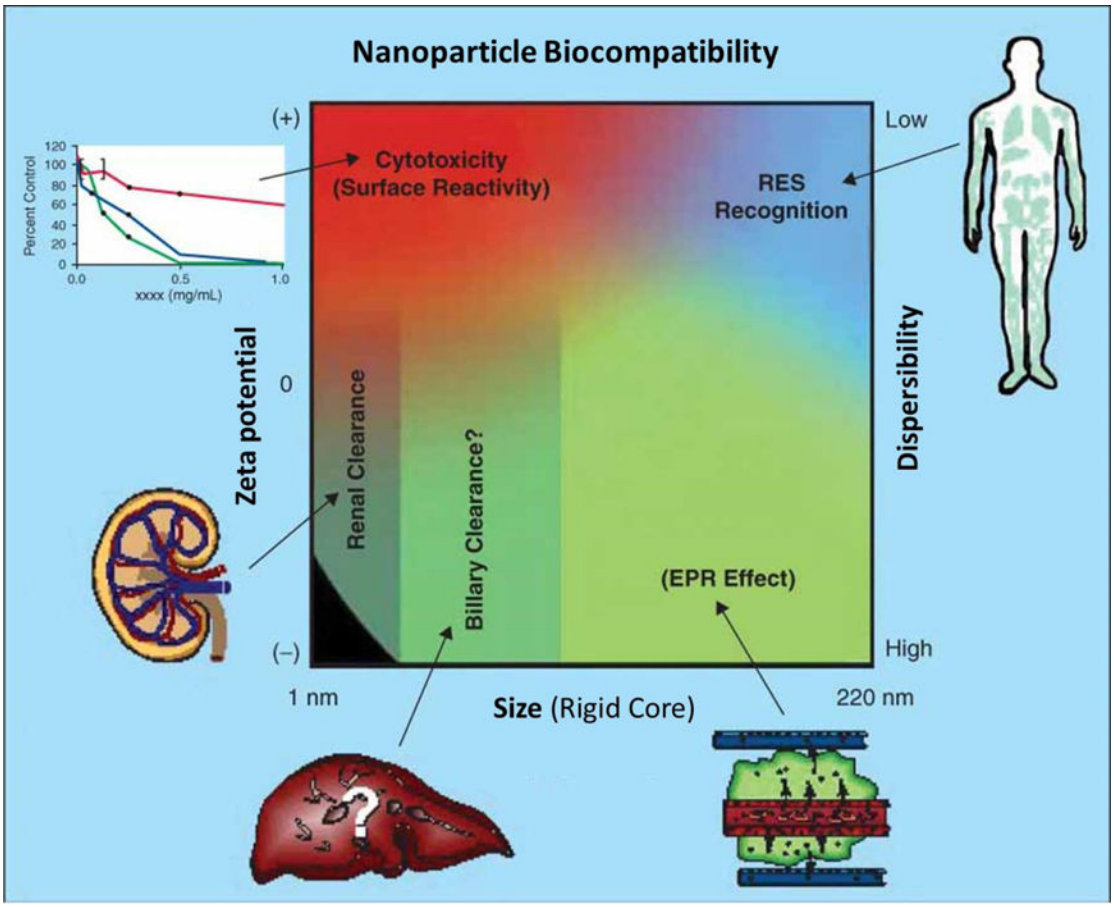

Figure 2.

The physicochemical characteristics (effect of size, zeta-potential, and dispersibility) of nanoparticles influence its biocompatibility. Qualitative trends in relationships between the independent variables of size (neglecting contributions from attached coatings and biologics), zeta potential (surface charge), and dispersibility with the route of uptake and clearance (shown in green), cytotoxicity (red), and RES recognition (blue). (Adapted from reference[65])

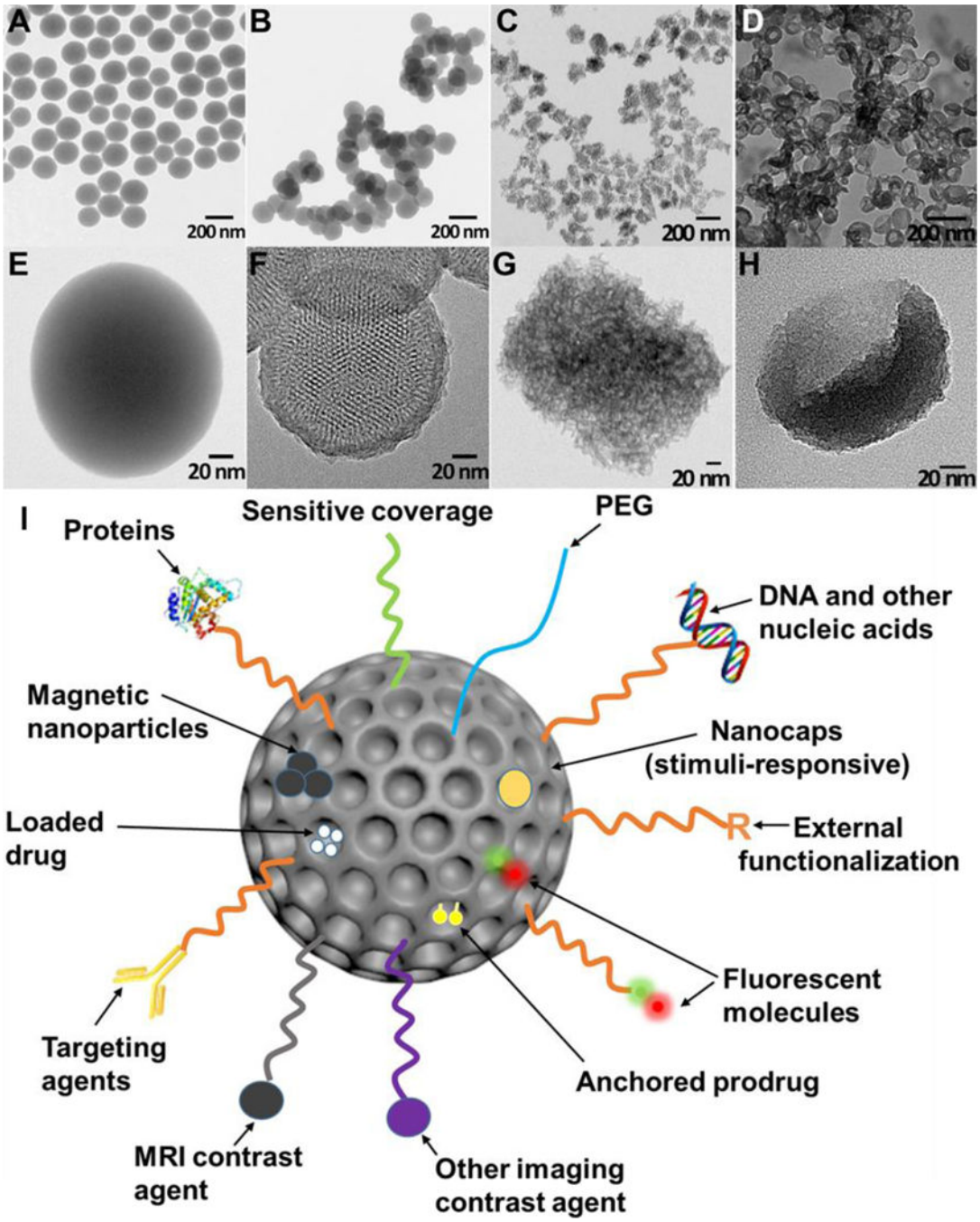

Figure 3.

TEM images of solid Stöber silica nanoparticles (A, E), MCM-41 mesoporous silica nanoparticles (B, F), mesocellular foam silica nanoparticles (C, G), and exosome-like silica nanoparticles (D, H) (Adapted from reference[31]). (I) Multifunctionality of silica nanoparticles. PEG is polyethylene glycol.

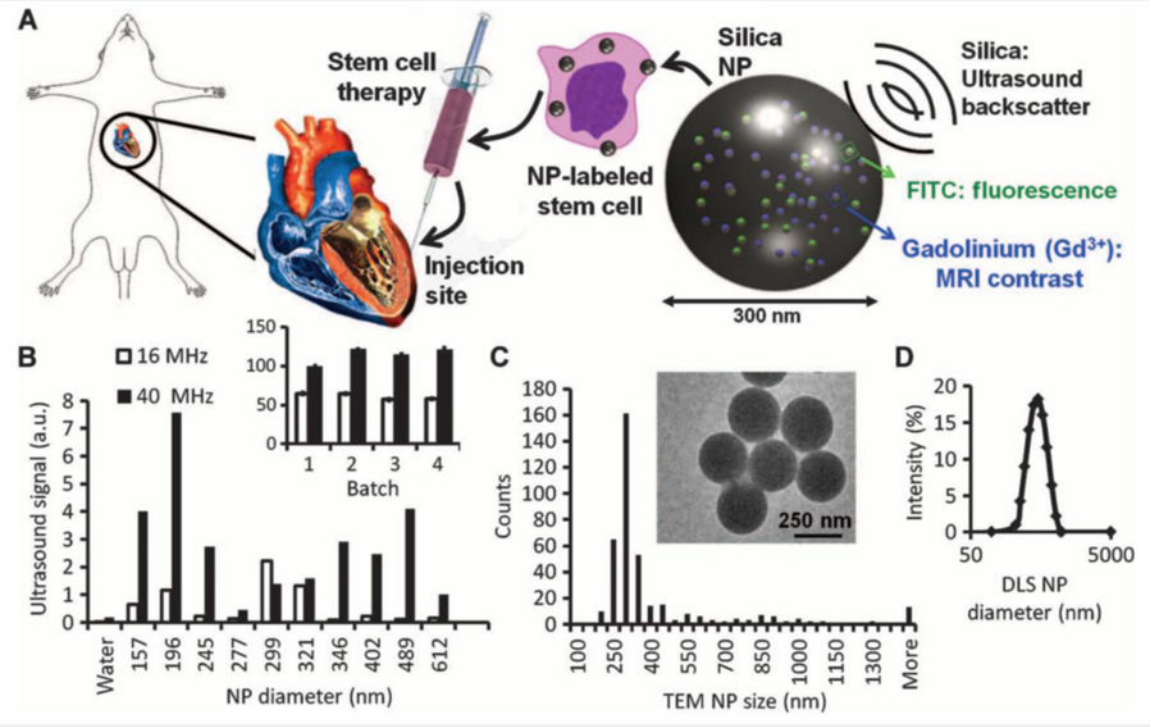

Figure 4.

(A) Cardiac stem cell therapy uses human mesenchymal stem cells loaded *ex vivo* with nanoparticles, which consist of silica (SiO_2) framework that backscatters ultrasound (black waves) and stabilizes Gd^{3+} and FITC fluorophores. (B) The ultrasound signals for 0.5 mg of different-sized NPs in an agarose phantom are shown at 40 and 16 MHz. Inset, batch-to-batch variability in ultrasound signal of 5 mg of NPs. (C) The size distribution within the 299-nm batch size selected from (B) had a mode size of 300 nm via TEM. Inset, TEM image of NPs. (D) Dynamic light scattering (DLS) of the 299-nm batch. Reproduced with permission[177]. Reprinted with permission from AAAS.

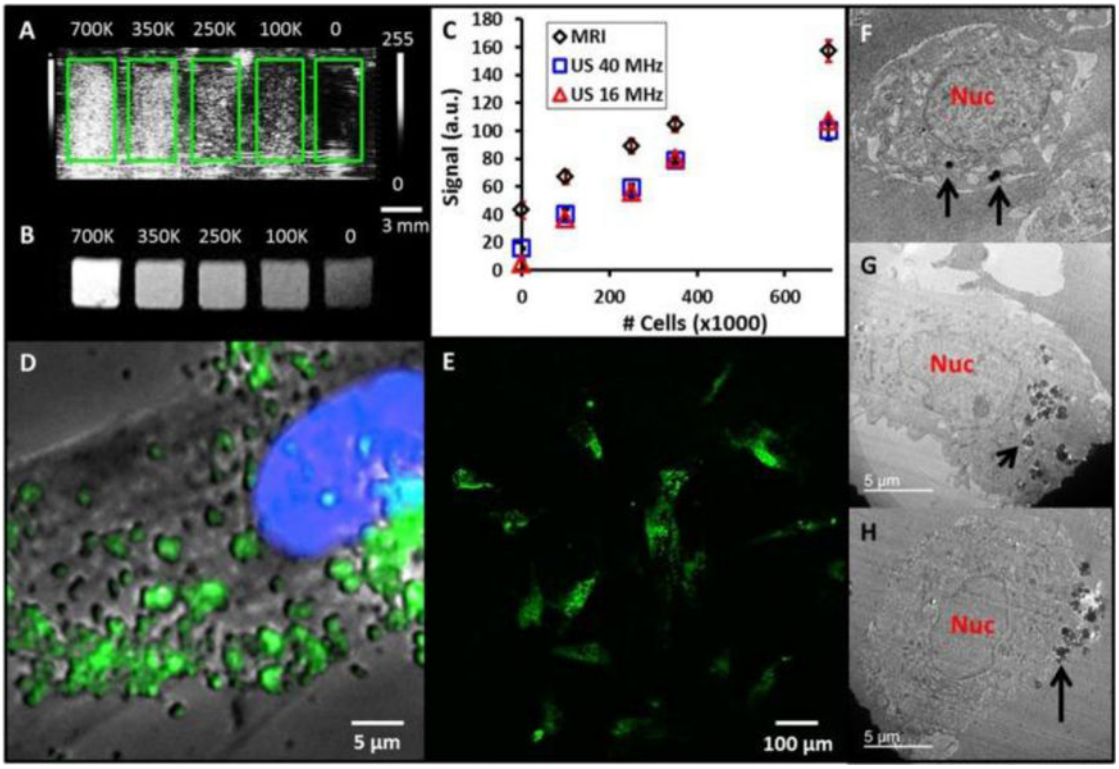

Figure 5.

(A) Coronal view of 40 MHz ultrasound imaging of decreasing number of MSNs-labeled mesenchymal stem cells (MSCs). Green boxes outline the boundaries of wells in the phantom. (B) Transverse view from T1-weighted MRI of the same cell sample. Scale bar and intensity bar to the right of A apply to both panels. (C) Dose response curves for increasing numbers of cells shows linear relationships at R^2 >0.97 for both MRI and ultrasound (US). (D) Epifluoresence microscopy with MSCs nucleus in blue and MSNs fluorescently tagged in green. Punctate areas are seen indicating endosomal accumulation of MSNs. (E) Confocal microscopy image indicating that the MSNs are located both on the cell periphery and interior. Panels (F-H) are three representative TEM images of MSCs labeled with MSNs. Note that the MSNs are located both on the cell periphery (F, H) and interior (G). Nuc: nucleus; Black arrows: MSNs. Reproduced with permission[113].

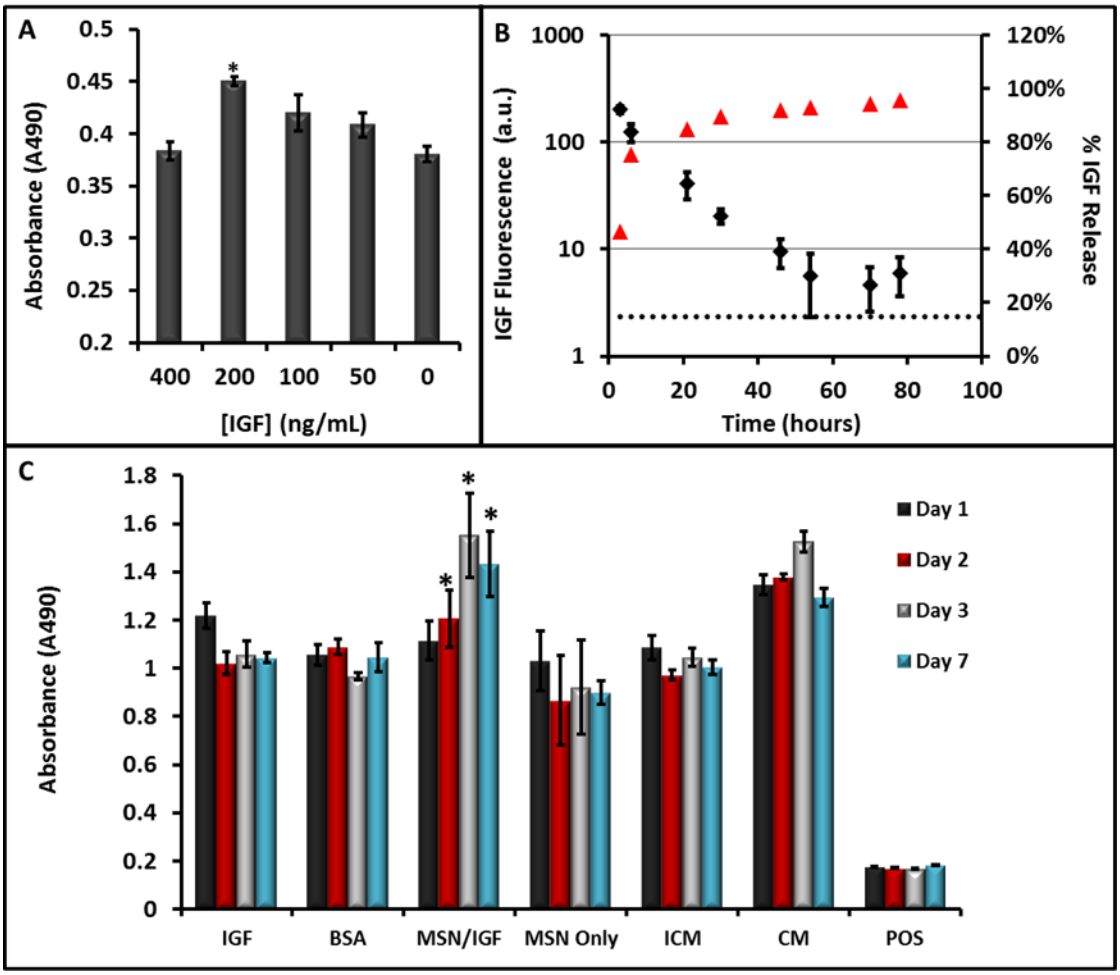

Figure 6.

(A) The ability of IGF to increase cell survival under serum-free conditions was studied at increasing concentrations of IGF—values of 200 ng/mL were optimal and significantly ($p<0.001$) increased viability 25% relative to untreated cells. (B) The release kinetics of IGF from the MSNs showed sustained release up to 48 hours. Here, red triangles are the percent of total release (right axis) and the black diamonds are absolute fluorescence from free IGF. (C) Sustained release of (IGF) from porous MSNs increases cell survival under serum-free media challenge as studied with MTS assay. The * indicates that the IGF-NPs had a statistically significant increase in viability versus incomplete media ($p<0.05$) and free IGF ($p<0.05$). IGF: Free IGF; BSA: Bovine Serum Albumin Control; MSNs/IGF: MSNs loaded with IGF; ICM: Incomplete Media (serum-free); CM: Complete Media. Error bars represent the standard error. Reproduced with permission[113].

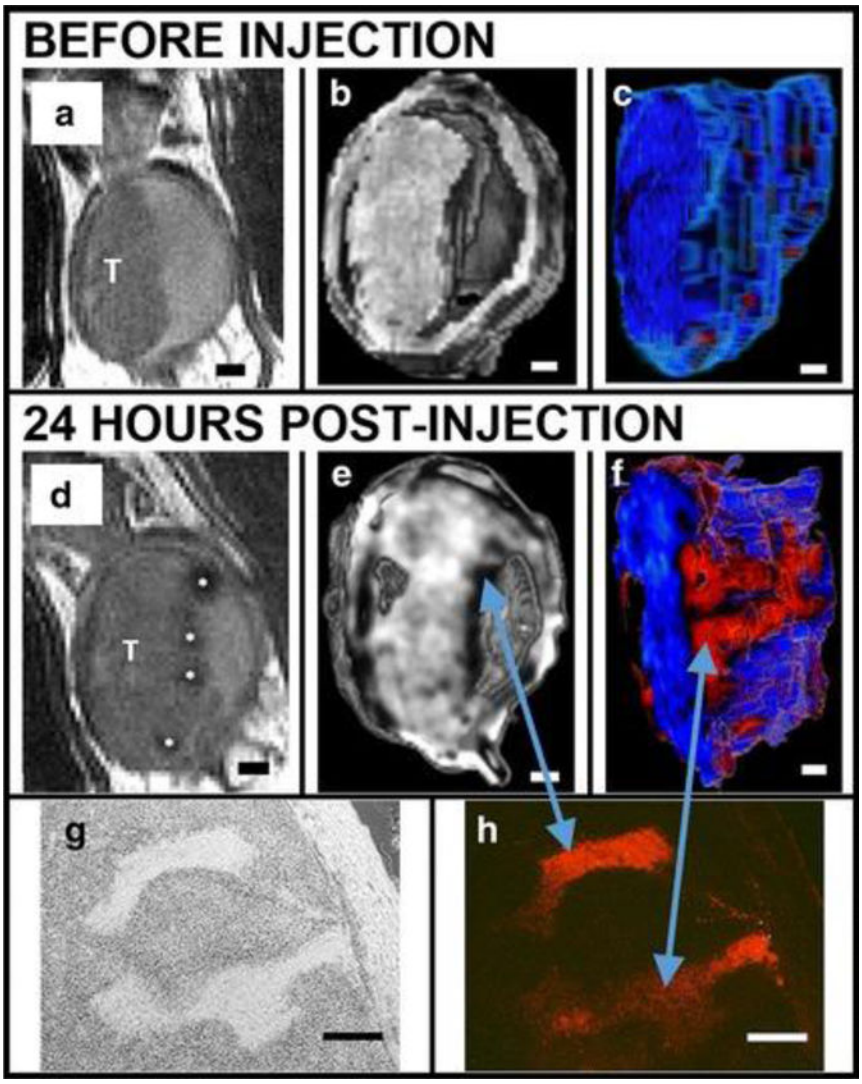

Figure 7.

MSNs bind preferentially to bladder cancer cells relative to normal bladder epithelia in vivo as shown in a series of renderings of T2-weighted MRI scans acquired before (A-C) and after (D-F) intravascular instillation of Gd_2O_3–TRITC–MSN. (A, D) 2D grayscale view, T: tumor. (B, E) Three-dimensional (3D) rendering images. (C, F) The tumor is segmented and rendered with a pseudo color map. Finger-like projections are revealed which are not observed before the injection of particles (C). Histology confirms anatomical observations and particle penetrations in the structures within the tumor: bright field (G) and fluorescent microscopy (H). Scale bars 1 mm (A-F); 250 μm (G, H). Reproduced with permission from Ref[180].

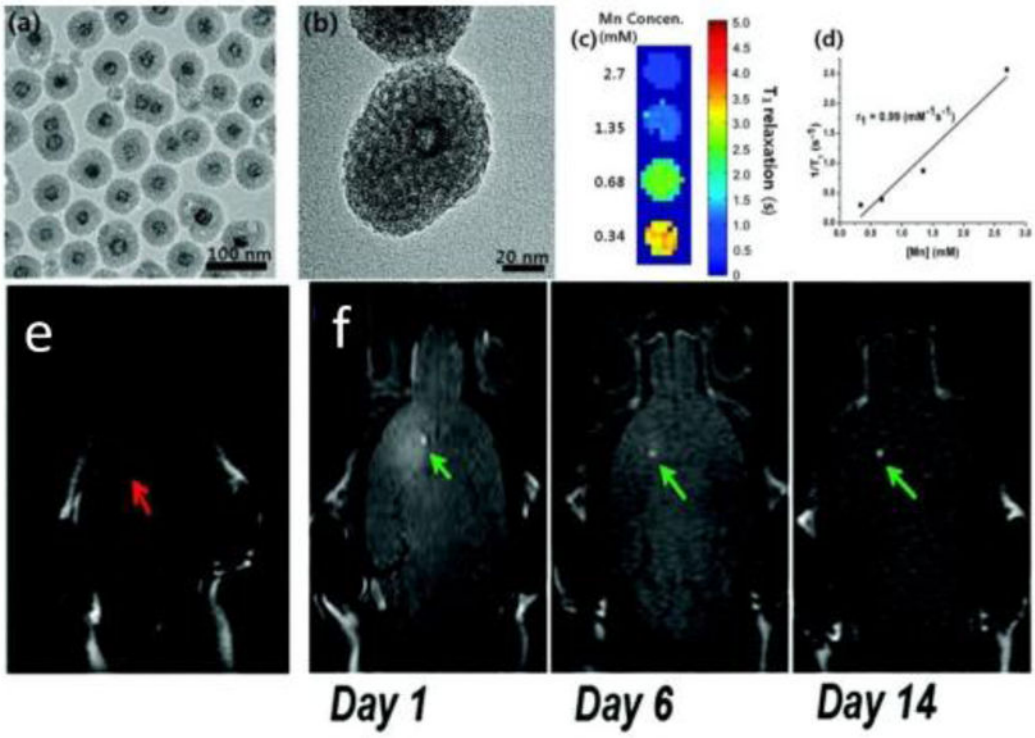

Figure 8.

(A) TEM image. (B) HRTEM image of a single nanoparticle. (C) T_1 map of HMnO@mSiO$_2$ nanoparticles suspended in water at 11.7 T. (D) Plot of $1/T_1$ versus Mn concentration. The slope indicates the specific relaxivity (r_1). (E) *In vivo* MRI shows no hyperintense signal (red arrow) was detected in mouse transplanted with unlabeled MSCs. (F) Hyperintense signals (green arrows) were detected in mouse transplanted with HMnO@mSiO$_2$-labeled MSCs and were still detectable 14 days after the injection. Reproduced with permission from Ref[50].

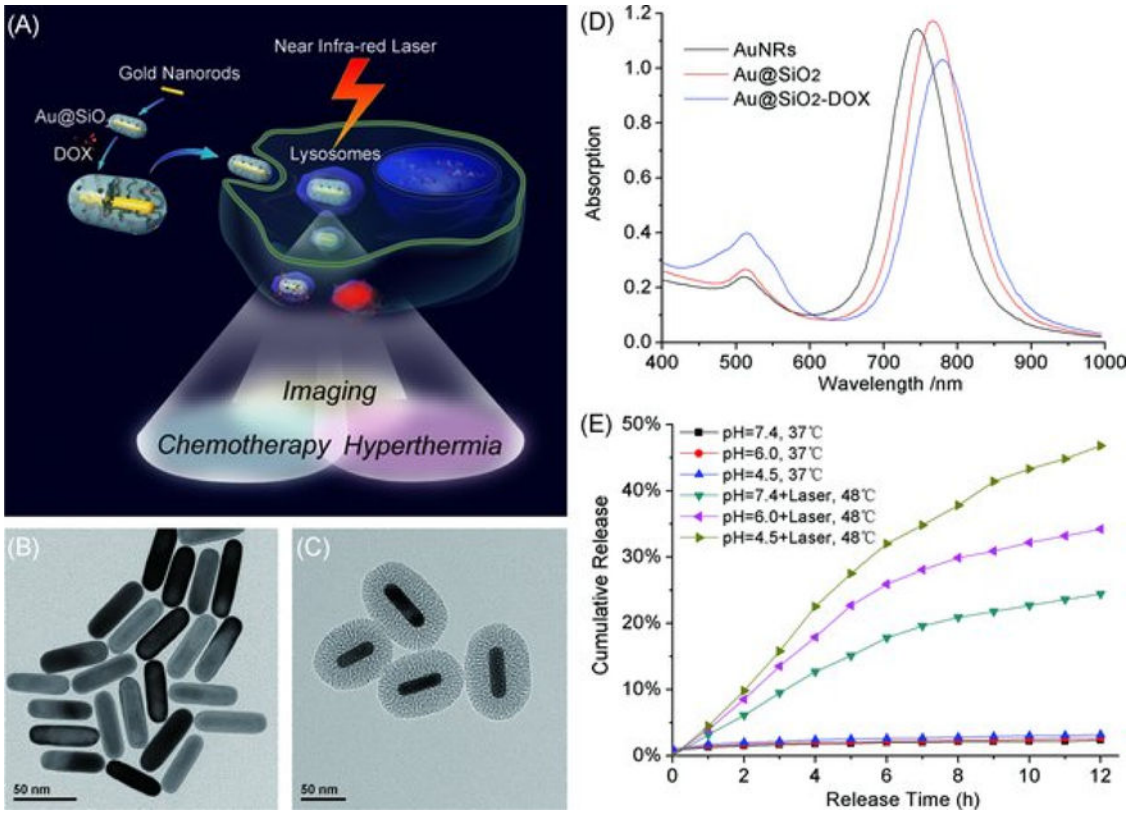

Figure 8.

(A) Schematic illustration of mesoporous silica-coated gold nanorods ($Au@SiO_2$) as a novel multifunctional theranostic platform for cancer treatment. TEM images of (B) AuNRs and (C) $Au@SiO_2$; (D) extinction spectra of AuNRs, $Au@SiO_2$, and $Au@SiO_2$–DOX, and (E) DOX release profiles from $Au@SiO_2$–DOX with and without near infrared (NIR) laser irradiation at different pH. Reproduced with permission from Ref[184].

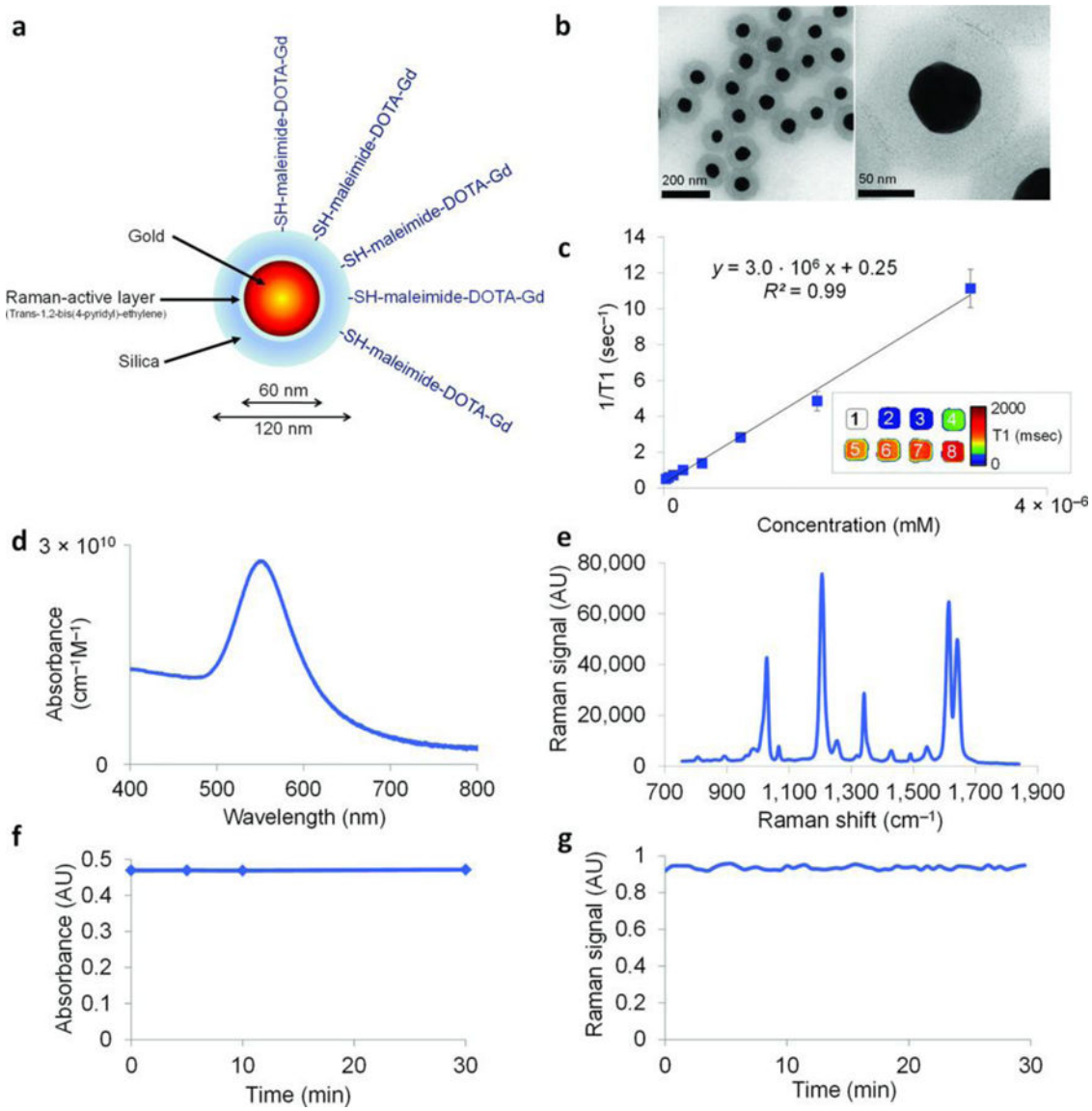

Figure 9.

Characterization of the NPs. (A) Simplified diagram: A 60 nm gold core is surrounded by a thin Raman active layer that is protected by a 30 nm silica coating. The silica coating was further functionalized with maleimide-DOTA-Gd, which was conjugated to the thiol group on the silica. DOTA, tetraazacyclododecane-1,4,7,10-tetraacetic acid, is a chelator. (B) Transmission electron microscopy images of NPs. (C) Particle relaxivity derived from T1 maps of probe dilutions in MRI phantoms. Data represent mean of two separate phantoms containing separate probe conjugations. Inset: T1 map of a MRI phantom containing NPs at concentrations ranging from 3.2 nM (1) to 25 pM (8). (D) Optical absorbance of NPs. (E) Raman spectrum of NPs with characteristic peaks at 1,021 cm^{-1}, 1,204 cm^{-1}, 1,340 cm^{-1}, 1,614 cm^{-1}, and 1,638 cm^{-1}. (F, G) During 30 min of continuous laser irradiation, the optical absorbance (F) and the Raman signal (G) remained constant. Adapted by permission from Macmillan Publishers Ltd: [Nature Medicine][185], copyright (2012).

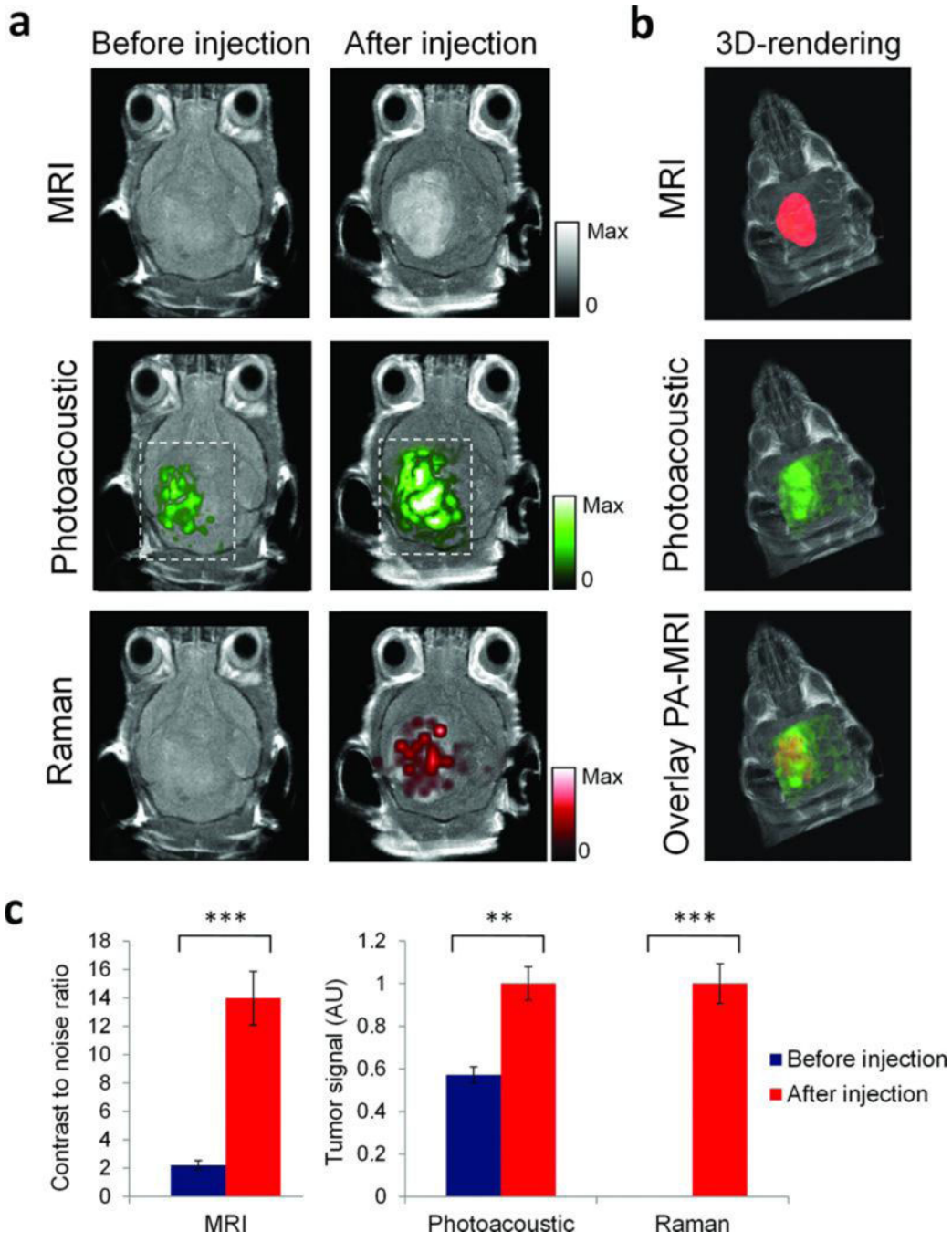

Figure 10.

Triple-modality detection of brain tumors in living mice with integrated nanoparticles. Three weeks after orthotopic inoculation, tumor-bearing mice (n = 4) were injected intravenously with the NPs. Photoacoustic, Raman, and MRI images of the brain (skin and skull intact) were acquired before and 2 h, 3 h, and 4 h after injection, respectively. (A) 2D axial MRI, photoacoustic, and Raman images. The post-injection images of all three modalities demonstrated clear tumor visualization. The photoacoustic and Raman images were co-registered with the MR image, demonstrating good co-localization between the three

modalities. (B) 3D rendering of MR images with the tumor segmented (red; top); overlay of 3D photoacoustic images (green) over MRI (middle); and overlay of MRI, segmented tumor and photoacoustic image (bottom) showing good co-localization of the photoacoustic signal with the tumor. (C) Quantification of signal in the tumor shows significant increase in MRI, photoacoustic and Raman signals before versus after the injection (*** indicates $P < 0.001$, ** indicates $P < 0.01$). Adapted by permission from Macmillan Publishers Ltd: [Nature Medicine][185], copyright (2012).

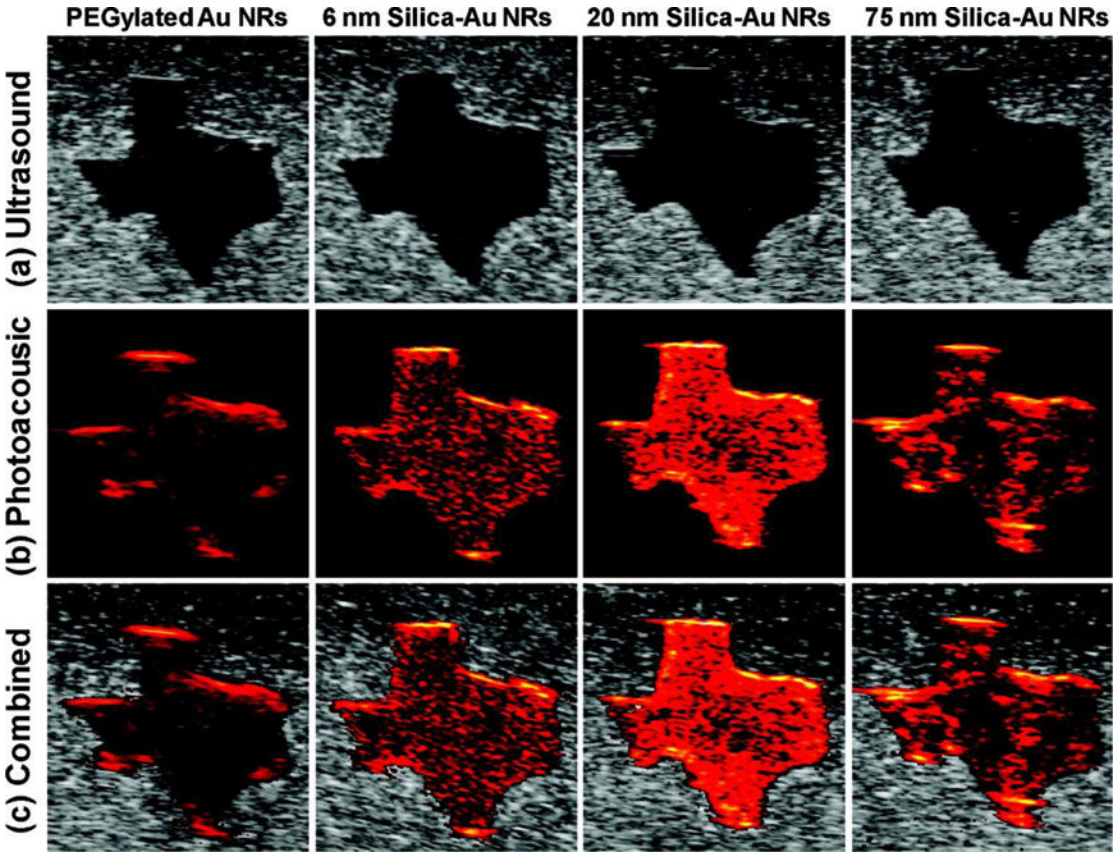

Figure 11.

(A) Ultrasound, (B) photoacoustic, and (C) combined ultrasound and photoacoustic images (top to bottom) of inclusions containing PEGylated AuNRs and gold−silica core−shell nanorods with 6 nm silica coating, 20 nm silica coating, and 75 nm silica coating (left to right). Each image covers a 6 mm by 6 mm field of view. Reproduced with permission from Ref[172]. Copyright (2011) American Chemical Society.

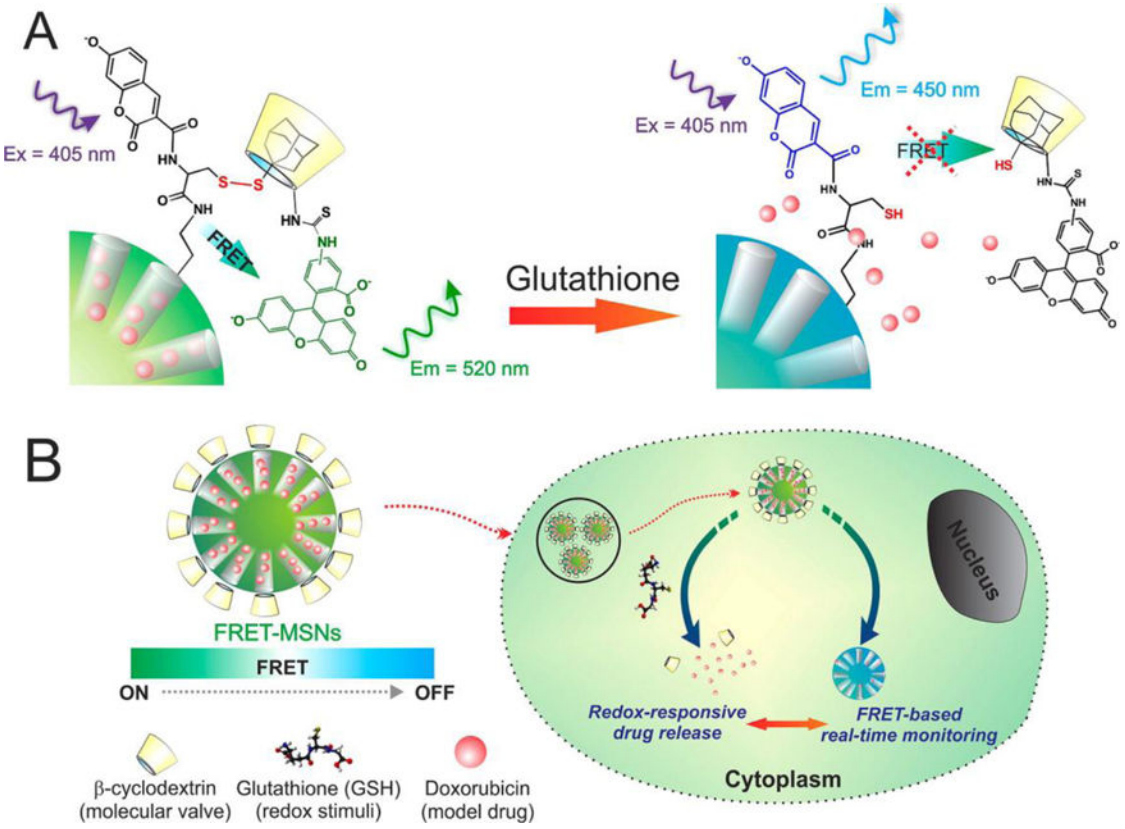

Figure 12.

Schematic representation of the redox responsive FRET-MSNs. (A) The coumarin-labeled cysteine on the surface of the FRET-MSNs acts as a donor and the FITC-β-CD acts as an acceptor thereby forming a FRET system when the disulfide bond is intact (left). The disulfide bond is cleaved in the presence of redox stimuli and then the molecular valve FITC-β-CD is removed from the surface of the MSNs. Thereby the FRET between coumarin and FITC is abolished. (B) The drug delivery is triggered by glutathione, rich in the cytoplasm of cancer cells. Simultaneously, change of FRET signal report the uncaging event and estimate the dosing amount of drug. Figure 1A is a magnified representation of Figure 1B, indicating the FRET system. Reproduced with permission from Ref[110]. Copyright (2013) American Chemical Society.

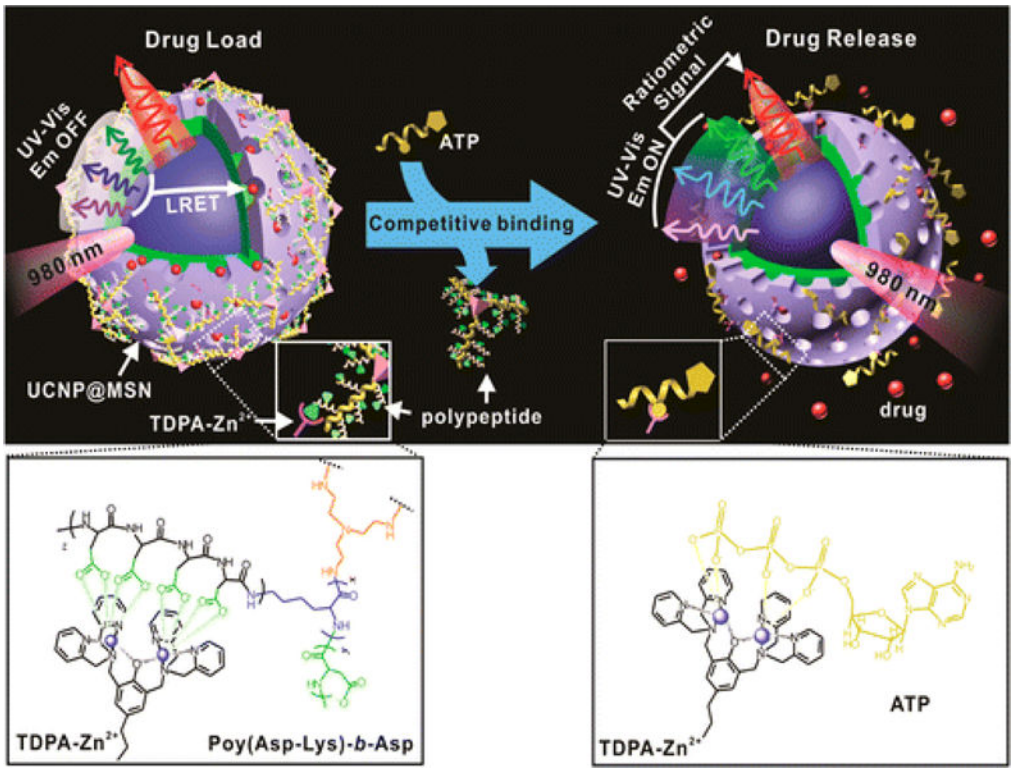

Figure 13.

Schematic representation of the real-time monitoring of ATP-responsive drug release from polypeptide wrapped TDPA-Zn^{2+}-UCNP@MSNs. Small molecule drugs were entrapped within the mesopores of the silica shell on the nanoparticle by branched polypeptide capping the pores through a multivalent interaction between the oligo-aspartate side chain in the polypeptide and the TDPA-Zn^{2+} complex on nanoparticles surface. The UV–visible emission from the multicolor UCNP under 980 nm excitation was quenched because of the LRET between the loaded drugs and the UCNP. The addition of small molecular nucleoside-polyphosphates such as ATP led to a competitive binding of ATP to the TDPA-Zn^{2+} complex, which displaced the surface bound compact polypeptide because of the high binding affinity of ATP to the metallic complex. The drug release was accompanied with an enhancement in the UV–visible emission of UCNP, which allows for real-time monitoring of the drug release *via* a ratiometric signal using the NIR emission of UCNP as an internal reference. Reprinted with permission from Ref[187]. Copyright (2015) American Chemical Society.

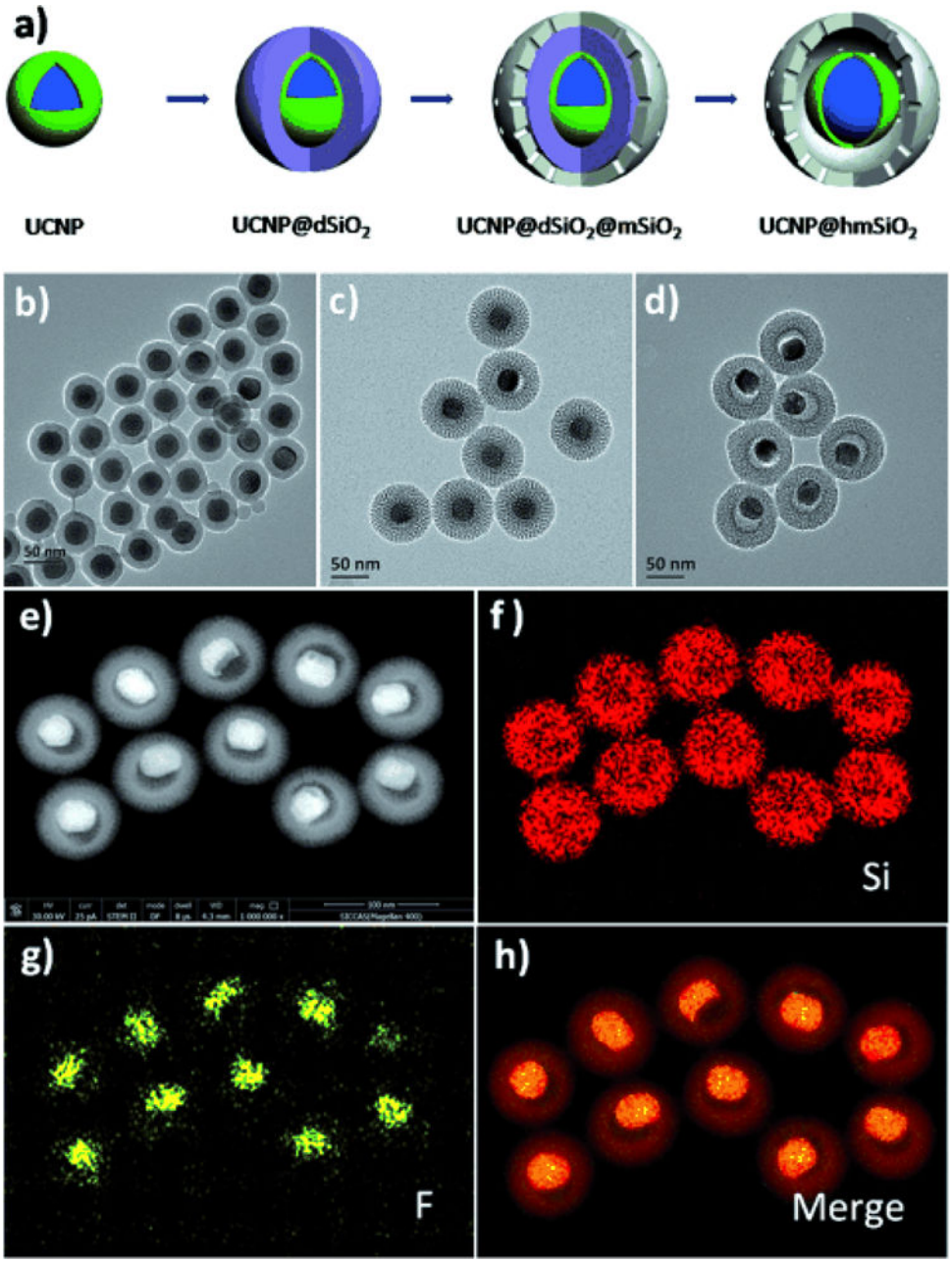

Figure 14.

(A) The formation process of the nanoparticles. (B-D) TEM images of (B) UCNP@dSiO$_2$, (C) UCNP@dSiO$_2$@mSiO$_2$, and (D) UCNP@hmSiO$_2$. (E-H) STEM images and corresponding elemental (F, Si) mappings of UCNP@hmSiO$_2$. Reproduced with permission from Ref[188].

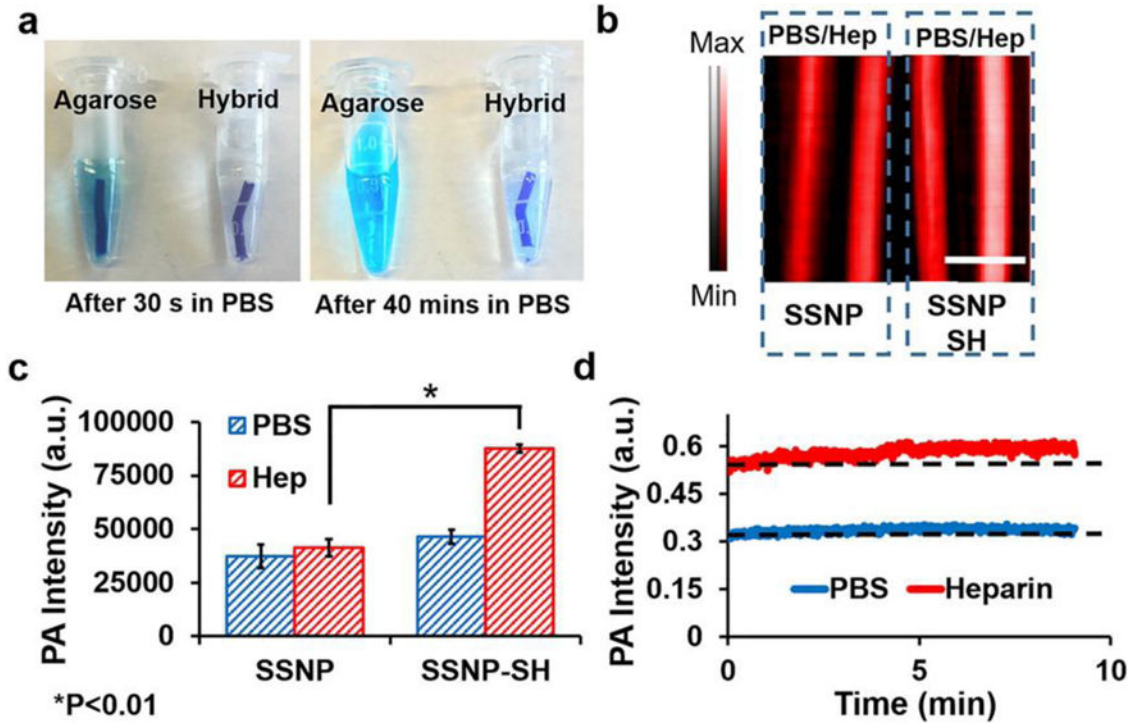

Figure 15.

Optimization of material for a heparin-responsive catheter. (A) Methylene blue in agarose was not stable with more than 40% methylene blue release in PBS after 40 min. The addition of nanoparticles for an integration reduced this release to less than 10%. (B) Photoacoustic images of methylene blue loaded on as-made silica nanoparticles (SSNP; −23 mV) and methylene blue loaded on thiol-coated silica nanoparticles (SSNP-SH; −15 mV). Both were treated with PBS and heparin (Hep) but only the thiol-coated nanoparticles were responsive to heparin. The lower ζ-potential facilitated the photoacoustic signal increase. (C) Methylene blue-loaded SSNP-SH treated with heparin offers significantly more signal than SSNP-SH treated with PBS or SSNP. (D) The nanoparticle/agar material was treated with PBS or 10 U/mL heparin and imaged at 680 nm for 9 min with no decrease in signal. Reproduced with permission from Ref[32]. Copyright (2016) American Chemical Society.

Table 1

The primary advantages, disadvantages, and main biological applications of common nanoparticle types. (CT: computerized tomography; MPI: magnetic particle imaging; MRI: magnetic resonance imaging; PAI: photoacoustic imaging[76]; PDT: photodynamic therapy; PTT: photothermal therapy; RES: reticuloendothelial system).

Nanomaterials	Advantages	Disadvantages	Biological Applications
Carbon nanotubes[3–6]	Extravasation, Small in one dimension	Toxic in certain formats, Non-biodegradable	Raman, PAI, Drug delivery
Graphene[7–10]	High thermal conductivity, Large surface area Flexible	Non-biodegradable, Poor dispersibility	Biosensors, PTT, Drug delivery, Optical imaging
Liposomes[11–14]	Excellent biocompatibility, Load both hydrophobic and hydrophilic cargos, Fuse with cells	Unstable storage, Rapid leakage of hydrophilic drugs, Low encapsulation efficiency	Ultrasound, Lipofection, Drug delivery
Dendrimers[15–19]	Precisely controlled morphologies, Homogeneity, High ligand density, Controlled degradation	Multistep synthesis, High cost	Drug delivery, Gene delivery, Blood substitution
Polymer nanoparticles[20–25, 77]	Biocompatibility, Wide variety, High encapsulation	Unstable structure, Drug leakage	Ultrasound, Drug delivery
DNA[59–62]	Exquisite size control, Functional designs	Unstable,	Drug delivery
Silica nanoparticles[28–34]	Tunable morphologies, Easy surface modification, Biocompatible, Biodegradable	Poor biodistribution	Ultrasound, Drug delivery, Define sentinel lymph nodes
Quantum dots[36–39]	Tunable emission, Single excitation, Small, Good biodistribution	Toxic components, Non-biodegradable	Optical imaging, PTT
UCNPs[40–44]	Narrow emission spectra, Long luminescence lifetime Chemically stable	Low brightness, Size, surface, and laser power density dependent quantum yield	Optical imaging, PTT, Photo-induced drug delivery, Biosensors
Superparamagnetic iron oxide nanoparticles[45–49]	MRI T**2**-weighted contrast, Stable, Biodegradable	Weak signal, High dose, RES accumulation	MRI, MPI, Hyperthermia, Directing, Separation
Other metal oxide nanoparticles[50–52]	Tunable morphology, Degradable	Poor biocompatibility	Antimicrobial agents, Drug delivery
Noble metals nanoparticles[54–58, 78]	Tunable, Stable, Inert, Thermally conductive, Plasmonic	Weak signal, High dose, Poor biodistribution, Non-biodegradable, Low drug loading	CT, PAI, PDT, PTT

Table 2

The most frequently used silanes used for surface modification on silica nanoparticles (NPs) and their functions.

Silanes	Function Group	Application
(3-aminopropyl)trimethoxysil ane (APTMS) (3-aminopropyl)triethoxysilan e (APTES)	$-NH_2$	Reduced aggregation[105], Fluorescent labeling[144], Surface charge modification[145], DNA binding and protection from enzymatic cleavage[149]
(3-mercaptopropyl)-trimethox ysilane (MPTMS)	−SH	Conjugate with maleimides[106], Thiol/disulfide exchange reactions to attach oligonucleotides[150], Surface charge modification[32, 151]
Polyethylene glycol-silane (PEG-silane)	−PEG	Increased circulation time[152], Reduced aggregation and increase particle dispersity in aqueous solution[127]
Alkylsilane	Alkyl chain	Hydrophobic coating[153], Increase ultrasound contrast[154]
Carboxyethylsilanetriol	−COOH	Functionalize silica NPs and provide reactive sites for amine[155]
3-trihydroxysilylpropyl methylphosphonate	$-PO_3-$	Functionalize silica NPs and provide reactive sites for amine[156]
(3-isocyanatopropyl)-triethox ysilane	−NCO	Functionalize silica NPs and provide reactive sites for amine[157]

Table 3

Functions of silica in integrated nanoparticles.

Formulations	Function
Silica core	High dielectric constant enhances light absorption[168], Therapeutic reservoir for drug delivery[158,169,170], Increase ultrasound contrast[129]
Silica shell	Facilitates functionalization of NPs surface[168,171], Amplifies photoacoustic signal[172], Therapeutic reservoir for drug delivery[173], Enhances colloidal and chemical stability of the core[174], Separates core from outside layer[175], Decreases cytotoxicity of core[160]
Silica matrix	Prevents photobleaching of fluorophores[144], Decreases cytotoxicity[113, 176, 177]